Activation of H_2O_2 over Zr(IV). Insights from Model Studies on Zr-monosubstituted Lindqvist Tungstates

Nataliya V. Maksimchuk,[†] *Vasilii Yu. Evtushok,*[†,‡] *Olga V. Zalomaeva,*[†] *Gennadii M. Maksimov,*[†,≠] *Irina D. Ivanchikova,*[†] *Yuriy A. Chesalov,*[†] *Ilia V. Eltsov,*[‡] *Pavel A. Abramov,*[#] *Tatyana S. Glazneva,*[†] *Vadim V. Yanshole,*[▽,‡] *Oxana A. Kholdeeva,*[†,*] *R. John Errington,*[§,*] *Albert Solé-Daura,*[‖] *Josep M. Poblet,*[‖] *and Jorge J. Carbó*[‖,*]

[†] Boreskov Institute of Catalysis, Pr. Lavrentieva 5, Novosibirsk 630090, Russia

[‡] Novosibirsk State University, Pirogova str. 2, Novosibirsk 630090, Russia

[#] Nikolaev Institute of Inorganic Chemistry, Pr. Lavrentieva 3, Novosibirsk 630090, Russia

[▽] International Tomography Center SB RAS, Institutskaya str. 3a, Novosibirsk 630090, Russia

[§] Chemistry, School of Natural and Environmental Sciences, Bedson Building, Newcastle University, NE1 7RU, UK

[‖] Departament de Química Física i Inorgànica, Universitat Rovira i Virgili, 43005 Tarragona, Spain

RECEIVED DATE

ABSTRACT. Zr-monosubstituted Lindqvist-type polyoxometalates (Zr-POM), $(Bu_4N)_2[W_5O_{18}Zr(H_2O)_3]$ (**1**) and $(Bu_4N)_6[\{W_5O_{18}Zr(\mu\text{-}OH)\}_2]$ (**2**) have been employed as molecular models to unravel the mechanism of hydrogen peroxide activation over Zr(IV) sites. Compounds **1** and **2** are hydrolytically stable and catalyze epoxidation of C=C bonds in unfunctionalized alkenes and α,β-unsaturated ketones, as well as sulfoxidation of thioethers. Monomer **1** is more active than dimer **2**. Acid additives greatly accelerate the oxygenation reactions and, oppositely, suppress H_2O_2 unproductive decomposition in the presence of **1** and **2**, thereby increasing oxidant utilization efficiency up to >99%. Product distributions are indicative of heterolytic oxygen transfer mechanism that involves electrophilic oxidizing species formed upon

[≠] Dr. Gennadii M. Maksimov passed away during the COVID-19 pandemic.

interaction of Zr-POM and H_2O_2. The interaction of **1** and **2** with H_2O_2, and the resulting peroxo derivatives, have been investigated by UV-vis, FTIR and Raman spectroscopy, HR-ESI-MS, and combined HPLC-ICP-AES technique. Also the interaction between an ^{17}O-enriched dimer, $(Bu_4N)_6[\{W_5O_{18}Zr(\mu\text{-}OCH_3)\}_2]$ (**2'**), and H_2O_2 was analyzed by ^{17}O NMR spectroscopy. Combining these experimental studies with DFT calculations suggested the existence of dimeric peroxo species $[(\mu\text{-}\eta^2\text{:}\eta^2\text{-}O_2)\{ZrW_5O_{18}\}_2]^{6-}$, as well as monomeric Zr-hydroperoxo $[W_5O_{18}Zr(\eta^2\text{-}OOH)]^{3-}$ and Zr-peroxo $[HW_5O_{18}Zr(\eta^2\text{-}O_2)]^{3-}$ species. Reactivity studies revealed that the dimeric peroxo is inert toward alkenes but is able to transfer oxygen atom to thioethers while the monomeric peroxo intermediate is capable of epoxidizing C=C bonds. DFT characterization of the reaction mechanism identifies monomeric Zr-hydroperoxo intermediate as the real epoxidizing species, and the corresponding α-oxygen transfer to the substrate as the rate-determining step. Calculations also showed that protonation of Zr-POM reduces significantly the free-energy barrier of the key oxygen-transfer step because of the higher electrophilicity of the catalyst, and that dimeric species hampers the approach of alkene substrates due to steric repulsions reducing its reactivity. The improved performance of Zr(IV)-catalyst relatively to Ti(IV) and Nb(V) catalysts is respectively due to a flexible coordination environment and to a low tendency to form energy deep-well, low-reactive Zr-peroxo intermediates.

KEYWORDS: *Epoxidation, DFT, hydrogen peroxide, Lindqvist tungstate, zirconium*

INTRODUCTION

The selective catalytic oxidation of organic compounds using low cost green oxidants is of both fundamental and practical interest.[1-4] Aqueous hydrogen peroxide is one of the most attractive oxidants from both ecological and economic aspects.[5-8] A range of microporous and mesoporous catalysts containing transition metal ions isolated in the framework of inorganic matrices or grafted

onto the surface have been prepared and examined in H_2O_2-based oxidations.[1-27] So far, titanium-[9-17] and niobium-containing[18-29] molecular sieves have been widely recognized as catalysts for selective oxidations with H_2O_2. Meanwhile, Zr-containing silicates also demonstrated a pronounced catalytic activity in H_2O_2-based oxidations.[30-38] Epoxides and diols most often predominated in the oxidation of alkenes.[31,32,34-36] However, in some cases, a significant amount of allylic oxidation products were also detected.[33,34]

In recent years, metal–organic frameworks (MOFs) have attracted great interest due to their potential applications in gas storage and separation, molecular recognition and drug delivery as well as heterogeneous catalysis.[39–48] Zr-containing MOFs have been reported as active and recyclable catalysts for oxidative transformations using H_2O_2 as oxidant.[48–58] Recently, some of us have found a remarkable effect of acid additives on selectivity of H_2O_2-based alkene oxidation over Zr-based metal-organic frameworks.[56,58] It was demonstrated that protons facilitate heterolytic activation of the oxidant and prevent its unproductive degradation on Zr-MOFs, thereby leading to selective oxygenation of the C=C bond without oxidation of allylic C-H bonds via a homolytic mechanism. However, the structure of the active peroxo zirconium species operating with Zr-MOFs remained unclear.

Despite the remarkable progress in surface science, investigation of mechanistic issues remains complicated in heterogeneous catalysis due to difficulties of the registration and identification of active catalytic species. Owing to their evident structural analogy with metal oxide surfaces and possibility of investigation at the atomic (molecular) level, polyoxometalates (POMs) have found applications as tractable molecular models for heterogeneous metal-oxide catalysts,[59,60] including single-site ones.[61-67] Moreover, a unique combination of properties, such as thermodynamic stability to oxidation and resistance to hydrolysis over a wide range of pH, tunable solubility, acidity and redox activity, made POMs the focus of a wide range of research areas.[68–81] Proust and co-workers suggested using Zr-containing Lindqvist-type polyoxotungstates as soluble

analogues of heterogeneous zirconia-supported tungsten catalysts.[82,83] Some of us have found similarities in the catalytic performance of Zr-monosubstituted Keggin-type POMs and mesoporous zirconium silicates.[84,85] These model studies based on the Keggin Zr-POMs revealed that the presence of acid protons is vital for their activity. While $(Bu_4N)_9[\{PW_{11}O_{39}Zr\}_2(\mu\text{-OH})(\mu\text{-O})]$ containing no acid protons reacted with neither H_2O nor H_2O_2 and showed minor catalytic activity in oxidations with H_2O_2, its protonated forms, $(Bu_4N)_8[\{PW_{11}O_{39}Zr(\mu\text{-OH})\}_2]$ and $(Bu_4N)_7H[\{PW_{11}O_{39}Zr(\mu\text{-OH})\}_2]$, revealed significant activity.[84] However, in contrast to Keggin Ti-POMs,[86-90] homolytic oxidation mechanism seemed to prevail with Keggin Zr-POMs, even after increasing the amount of protons.[84,85] Nomiya et al. have also tested several Zr/Hf-containing Keggin and sandwich POMs as catalysts on the epoxidation of cyclooctene with H_2O_2, but they decomposed under reaction conditions, or gave moderate/no activity.[91]

Recently, we have shown that Ti- and Nb-monosubstituted tungstates of the Lindqvist structure, $(Bu_4N)_3[(CH_3O)TiW_5O_{18}]$ and $(Bu_4N)_2[(CH_3O)NbW_5O_{18}]$, are more active and selective than their Keggin type analogues and display catalytic performances similar to those of heterogeneous Ti- and Nb-containing catalysts in alkene epoxidation with hydrogen peroxide.[92,93] Using Lindqvist Ti- and Nb-POMs as molecular models, and combining kinetic, spectroscopic, and computational techniques, we were able to provide insight into the reaction mechanism, to rationalize the differences in the catalytic performances of Ti and Nb single-site catalysts, and to elucidate the role of protons in H_2O_2 activation. Here, we turn our attention to the H_2O_2 activation over Zr(IV), aiming to gain insights into the reaction mechanism and to establish structure–reactivity relationships. To this end, Zr-monosubstituted tungstates of the Lindqvist structure, $(Bu_4N)_2[W_5O_{18}Zr(H_2O)_3]$ (**1**) and $(Bu_4N)_6[\{W_5O_{18}Zr(\mu\text{-OH})\}_2]$ (**2**), as well as $(Bu_4N)_6[\{W_5O_{18}Zr(\mu\text{-}OCH_3)\}_2]$ (**2'**) enriched with ^{17}O, were investigated by means of specific product tests, kinetic, spectroscopic, and computational techniques.

EXPERIMENTAL SECTION

Instrumentation and Methods. The interaction of Zr-POM with H_2O_2 and MPS was studied by in situ IR spectroscopy using Alpha II spectrometer (Bruker) with Platinum Diamond ATR module in the range of 400–4000 cm^{-1} with a resolution of 4 cm^{-1} and accumulation of 32 scans. ATR-FTIR spectra (4000–350 cm^{-1}, 40 scans, resolution 4 cm^{-1}) were obtained using a Cary 660 FTIR spectrometer (Agilent Technologies) and a PIKE Technologies GladiATR accessory (diamond crystal). Raman spectra were measured in the backscattering geometry using a Horiba Jobin Yvon Lab-Ram HR spectrometer equipped with a N_2-cooled CCD- 2048 ×512 detector coupled to an Olympus BX41 microscope. Excitation was supplied by an argon ion laser (λ = 488 nm) with 4 cm^{-1} spectral resolution. Electronic absorption spectra were run on a Cary–50 spectrophotometer using a 0.2 cm quartz cells.

^{17}O and ^{1}H NMR spectra were recorded on a Bruker Avance 300 spectrometer operating at 300.0 (^{1}H) or 67.8 (^{17}O) MHz using 5 mm o.d. glass NMR tubes (0.5 mL solution volume). ^{1}H NMR spectra were referenced to residual CHD_2CN at δ 1.97 ppm in CD_3CN solvent. ^{17}O NMR spectra were referenced to external H_2O. ^{183}W and ^{31}P NMR spectra were recorded on a Bruker Avance III 500 spectrometer operating at 20.83 MHz (^{183}W) or 202.42 MHz (^{31}P) using 10 (^{183}W) or 5 (^{31}P) mm o.d. glass NMR tubes and referenced to external K_2WO_4 and 85% H_3PO_4 (δ 0 ppm), respectively.

GC analyses were performed using a gas chromatograph Tsvet-500 equipped with a flame ionization detector and a quartz capillary column (30 m×0.25 mm) filled with Agilent DB–5MS or Chromos GH-1000 gas chromatograph equipped with a flame ionization detector and a quartz capillary column (30 m × 0.25 mm) filled with BPX5. GC–MS analyses were carried out using an Agilent 7000B system with a triple–quadrupole mass–selective detector Agilent 7000 and a GC Agilent 7890B apparatus (quartz capillary column 30 m × 0.25 mm / HP–5MS).

Combined HPLC-ICP-AES studies were performed with HPLC system Milichrom A-02 (EcoNova, Russia) equipped with a two-beam spectrophotometric detector at the wavelength range

of 190−360 nm in ion-pair mode of reversed phase chromatography (ProntoSIL 120-5-C18AQ, 2x75 mm), eluents: A – 0.04% aqueous Bu_4NPF_6, B – acetonitrile (flow rate 0.2 mL min^{-1}, detection wavelength 270 nm). An ICP-AES spectrometer iCap 6500 Duo (Thermo Scientific, USA) with concentric nebulizer was applied as detector in hyphenated HPLC-ICP-AES mode. For quantitative estimations, the Zr 339.1 nm, W 239.7 nm spectral lines were selected. All measurements were performed in three replicates. The data acquisition and processing was carried out with iTEVA (Thermo Scientific, USA) software. In order to eliminate plasma quenching, the liquid coming out of the column into the spray chamber was diluted with deionized water. The concentrations of C, H, and N were determined with a CHNSO analyzer Vario EL Cube (Elementar Analysensysteme GmbH).

High-resolution electrospray ionization mass spectra (HR-ESI-MS) were obtained using ESI quadrupole time-of-flight high-resolution mass spectrometer Maxis 4G (Bruker Daltonics, Germany) with a direct injection of liquid samples. The spectra were recorded in the 300–3000 m/z range in negative mode.

Synthesis and Characterization of POMs. The syntheses of POMs enriched in ^{17}O were carried out under an atmosphere of dry, oxygen-free nitrogen using Schlenk and dry-box techniques.[94]

$(Bu_4N)_2[W_5O_{18}Zr(H_2O)_3]$ (**1**). The synthesis of a tetrabutylammonium salt of $[W_5O_{18}Zr(H_2O)_3]^{2-}$ was adapted from ref.[83]. A hydrogen sulfate buffer was prepared by the addition of H_2SO_4 to 1 *M* Na_2SO_4 solution until pH 2 was reached. $ZrOCl_2 \cdot 8H_2O$ (0.644 g, 2 mmol) was dissolved in 250 mL of the hydrogen sulfate buffer. The resulting solution was then diluted to 400 mL with distilled water (solution **A**). A second solution was prepared by dissolving 10.6 mmol of $Na_2WO_4 \cdot H_2O$ (3.30 g) in 35 mL of water. This solution was heated to boiling and then 4 mL of 5 *M* hydrochloric acid was added dropwise under vigorous stirring. The solution was cooled in an ice bath (solution **B**). The cold solution **B** was added to solution **A** under stirring and the mixture was

allowed to stand at room temperature for 3 days; 5.88 g of tetrabutylammonium bromide was then added, resulting in the fast precipitation of $(Bu_4N)_2[W_5O_{18}Zr(H_2O)_3]$. IR (1000–400 cm^{-1}): 962 (s, W=O), 883 (m), 832 (sh), 813 (s, WOW), 739 (sh), 690 (w), 665 (w), 636 (w), 592 (w), 420 (s). Raman (cm^{-1}): 978 (vs), 958 (sh), 909 (m), 882 (m), 850 (m).

The synthesis of $(Bu_4N)_6[\{W_5O_{18}Zr(\mu\text{-}OH)\}_2]$ (**2**) was carried out following the literature protocol.[83] Anal. Calcd (%) for $C_{96}H_{218}N_6Zr_2W_{10}O_{38}$: C, 28.20; H, 5.33; N, 2.06; O, 14.88; Zr 4.47; W, 44.99. Found: C, 27.70; H, 5.57; N, 2.02; Zr, 4.58; W, 43.7. IR (1000 - 400 cm^{-1}): 970 (sh, W=O), 945 (s, W=O), 881 (m), 812 (br, WOW), 731 (s, ZrOH), 645 (m), 625 (m), 557 (m), 430 (s), 419 (sh). Raman (cm^{-1}): 978 (vs), 954 (s), 914 (m), 888 (m), 839 (m). ^{183}W NMR (ppm, in CD_3CN): 50.8 ($4W_{eq}$), 78.2 ($1W_{ax}$).

$(Bu_4N)_2[W_6O_{19}]$ (**W_6**) enriched in ^{17}O was prepared and characterized as described elsewhere.[95] A solution of $(Bu_4N)_2WO_4$ (0.45g, 0.61 mmol) and $WO(OMe)_4$ (1.00 g, 3.08 mmol) in acetonitrile (6 mL) was treated with ^{17}O enriched water (110 μL) with thorough mixing. The resulting reaction mixture was left under stirring at 70 °C overnight. After cooling to -20 °C, white solid was isolated and dried in vacuo (0.36 g, 61%). ^{17}O NMR (ppm, in CH_3CN): 778.1 (W=O), 416.7 (WOW).

The heterometalate $(Bu_4N)_6[\{W_5O_{18}Zr(\mu\text{-}OCH_3)\}_2]$ (**2'**) enriched in ^{17}O has been synthesized by a method similar to that previously described for $(Bu_4N)_3[(CH_3O)TiW_5O_{18}]$[96] that involved initial degradation of **W_6** with $(Bu_4N)OH$ and subsequent addition of $Zr(OPr^i)_4(Pr^iOH)$ in dry acetonitrile using 40% ^{17}O-enriched water (H_2O^*) according to the following stoichiometry:

$$5\ [W_6O_{19}]^{2-} + 8\ OH^- + 5\ H_2O^* \rightarrow 6\ \text{“}[W_5O_{18}H_3]^{3-}\text{”} \quad (1)$$

$$\text{“}[W_5O_{18}H_3]^{3-}\text{”} + Zr(OPr^i)_4(Pr^iOH) \rightarrow [(Pr^iO)ZrW_5O_{18}]^{3-} + 4\ Pr^iOH \quad (2)$$

$$[(Pr^iO)ZrW_5O_{18}]^{3-} + CH_3OH \rightarrow [(CH_3O)ZrW_5O_{18}]^{3-} + Pr^iOH \quad (3)$$

$$2[(CH_3O)ZrW_5O_{18}]^{3-} \rightarrow [\{W_5O_{18}Zr(\mu\text{-}OCH_3)\}_2]^{6-} \quad (4)$$

$(Bu_4N)_2[W_6O_{19}]$ (500 mg, 0.26 mmol) was placed into Schlenk flask (solution **C**) and dissolved in 5 mL of CH_3CN under stirring at room temperature. Bu_4NOH (0.45 mL as 0.98 *M* solution in methanol) was placed into another Schlenk flask (solution **D**), and the solvent (CH_3OH) was pumped out and replaced to dry CH_3CN (this procedure was repeated 3 times). Then, solution **D** was transferred via cannula into solution **C**, and resulting pale blue reaction mixture was stirred overnight at room temperature. The resulting solution was transferred via cannula into a Schlenk flask containing $Zr(OPr^i)_4(Pr^iOH)$ (105 mg, 0.32 mmol) and left to stir for 2 h at room temperature. After that, 5 mL of H_2O* was added, and the resulting reaction mixture was left to stir for another 2 h at room temperature. Then, the volatiles were pumped dry and the solid was dissolved in 4 mL of CH_3CN and 0.5 mL of CH_3OH. The resulting solution was stirred overnight at room temperature, and then the volatiles were pumped dry. The resulting white solid was washed with ether, dried at room temperature, and then recrystallized from CH_3CN. Yield: 300 mg, 46%. ^1H NMR (ppm, in CD_3CN): 3,79 (s, 6H, OCH_3), 3.24 (t, 48H, NCH_2), 1.71 (m, 48H, CH_2), 1.48 (m, 48H, CH_2), 1.01 (t, 72H, CH_3). ^{17}O NMR (ppm, in CD_3CN): 712 (W=O), 692 (W=O), 486 (ZrOW), 387 (WOW), 378 (WOW), and –57 (μ_6-O).

Isolation and Characterization of Zr Peroxo Species. A number of zirconium peroxo species were prepared by the addition of 5, 10, 20, 35 or 50 equivalents of aqueous (30, 50 or 77%) H_2O_2 to a solution containing 100 mg of **2** in 0.6 mL of CH_3CN (see Table 1 for details). The colorless clear solution was stirred for 20 min at room temperature and diluted with 10 mL of ether. The resulting white solid was isolated by filtration, washed with ether and acetone and dried under Ar flow at room temperature. Likewise, two zirconium peroxo species were synthesized following a similar procedure by the addition of 20 or 40 equivalents of 30% H_2O_2 to a solution containing 100 mg of **1** in 0.6 mL of CH_3CN (see Table 1 for details, compounds **8** and **9**). The resulting peroxo species were characterized by ATR-FTIR, Raman, UV-vis, ^{183}W NMR, HR-ESI-MS, and HPLC-

ICP-AES technique. The amount of peroxo groups was estimated by titration with PPh_3 followed by monitoring with ^{31}P NMR[97] and GC.

Table 1. **The Ratio of Reagents Used in the Syntheses Zr-peroxo Species**

Peroxo species	Reagents			
	Zr-POM		H_2O_2,	
	type	mmol	% in water	mmol (equiv.[a])
3[b]	**2**	0.025	30	0.25 (5)
4	**2**	0.025	30	0.5 (10)
5	**2**	0.025	30	1.0 (20)
6	**2**	0.025	30	1.75 (35)
7	**2**	0.025	30	2.5 (50)
8	**1**	0.049	30	1.0 (20)
9	**1**	0.049	30	2.0 (40)
10	**2**	0.025	50	1.75 (35)
11	**2**	0.025	77	1.75 (35)

[a]Equivalents per moles of Zr in POM molecule. [b]Anal. Calcd (%) for $C_{96}H_{216}N_6Zr_2W_{10}O_{38}$: C, 28.20; H, 5.33; N, 2.06; Zr 4.47; W, 45.00. Found: C, 28.27; H, 5.60; N, 2.09; Zr, 4.40; W, 44.50.

Full details on the catalytic and stoichiometric oxidation reactions, interaction of POMs with H_2O and H_2O_2, as well as computational methodology are provided in the Supporting Information (SI).

RESULTS AND DISCUSSION

Catalytic Performance of Zr-POMs in Alkene Oxidation. Catalytic properties of the Lindqvist type dimers **2** and **2'** as well as monomer **1** were first assessed in the oxidation of cyclohexene (CyH) with hydrogen peroxide using an equimolar amount of the oxidant. CyH possesses highly reactive H atoms in the allylic position, which can be easily abstracted by radical species. Hence, the formation of allylic oxidation products, viz. cyclohexenyl hydroperoxide (HP), 2-cyclohexene-1-ol (enol), and 2-cyclohexene-1-one (enone), is a clear indication of a homolytic oxidation mechanism (Scheme

1).[98] Contrarily, the selective formation of epoxide along with the ring opening product *trans*-cyclohexane-1,2-diol (diol) and its overoxidation product 2-hydroxycyclohexanone (ketol) points to a heterolytic oxidation mechanism (Scheme 1).

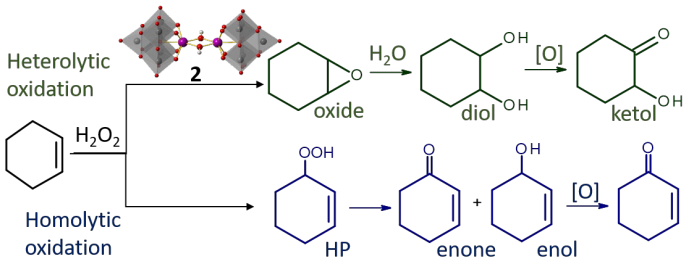

Scheme 1. Cyclohexene oxidation products formed via heterolytic or homolytic pathways in the presence of **2**.

In the presence of **2**, CyH conversion attained 35% after 1.5 h at 50 °C and then stopped. Total selectivity toward heterolytic oxidation products (epoxide, diol, and ketol) and efficiency of hydrogen peroxide utilization were 82% and 56%, respectively (Table 2, entry 1). Epoxide prevailed among the oxidation products. The methoxido form **2'** exhibited similar catalytic properties (Table 2, entry 7). In agreement with the previous results,[92] the Zr-free tungstate $(Bu_4N)_2[W_6O_{19}]$ was almost inactive in this reaction, indicating that the substitution of W(VI) for Zr(IV) is indispensable for the observed activity (Table 2, entry 10). The reaction in the presence of **2** was greatly accelerated with the addition of 1 equiv. of acid (Figure 1a). Moreover, CyH conversion and H_2O_2 utilization efficiency increased significantly, reaching the values of 75 and >99%, respectively (Table 2, entry 2). It is noteworthy that a similar trend was observed recently for Nb-containing Lindqvist-type POM[92] and Zr-containing MOFs.[56,58] Also, for Ti-containing POMs the addition of acidic protons accelerated the reaction and increased the selectivity towards the heterolytic products in alkene oxidation with H_2O_2.[99] Even minor (0.1 equiv. per Zr) additives of acid produced a pronounced effect on CyH oxidation rate and selectivity in the presence of **2** (Figure 1a, Table S1). If 1 equiv. of acid was used as the sole catalyst, the selectivity toward heterolytic oxidation products (epoxide and

diol) increased relative to the blank experiment (Table 2, compare entries 8 and 9), but the substrate conversion was insignificant relative to the POM-catalyzed reaction. Interestingly, the addition of 1 equiv of Bu_4NOH practically deactivated the catalyst **2** (Table 2, entry 3). Surprisingly, the use of 0.1 *M* H_2O_2 instead of 0.2 *M* gave a result close to the blank experiment (Table S2) and the addition of water to the reaction mixture did not change the result markedly (Table S2), indicating that namely concentration of the oxidant is critical to form the active (hydro)peroxo intermediate.

Table 2. **CyH Oxidation with H_2O_2 in the Presence of Zr-POMs.**[a]

Entry	Catalyst	Time,[b] h	CyH conv,%	TOF,[c] min^{-1}	H_2O_2 eff,[d] %	Product selectivity,[e] %				
						epoxide	diol	ketol	enol	enone
1	**2**	1.5	35	0.3	56	39	29	14	6	9
2	**2** + H^+	0.3	75	2.3	>99	9	57	29	4	0.5
3	**2** + OH^-	1.5	4	n.d.[f]	n.d.	33	15	0	17[g]	traces
4	**1**	0.3	54	1.0	70	17	54	25	2	2
5	**1** + H^+	0.3	75	2.5	>97	11	55	29	3	1
6	**1** + OH^-	1.5	40	0.7	n.d.	31	34	23	6	5
7	**2'**	1.5	35	0.3	n.d.	39	29	12	9	10
8	–[h]	5	5	n.d.	n.d.	21	traces	0	33	11
9	H^+	5	8	n.d.	n.d.	25	44	0	25	traces
10	$\mathbf{W_6}$	5	2	n.d.	n.d.	traces	0	0	traces	traces
11	**6**	0.3	52	n.d.	n.d.	20	54	19	4	3

[a]Reaction conditions: 0.004 *M* Zr, 0.2 *M* CyH, 0.2 *M* H_2O_2 (taken as 30% solution in water), 0.004 *M* $HClO_4$ or Bu_4NOH (if any), CH_3CN 1 mL, 50 °C. [b]Optimal reaction time to reach the maximum selectivity and conversion. [c]TOF = (moles of substrate consumed)/(moles of Zr × time), determined by GC from initial rates of substrate consumption. [d]H_2O_2 utilization efficiency = total yield of products based on the oxidant consumed. [e]Based on substrate consumed. [f]Hereinafter n.d. means not determined. [g]Cyclohexenyl hydroperoxide (33%) was also formed. [h]Blank experiment with no catalyst present.

Monomer **1** was evidently more active than dimer **2** and enabled higher CyH conversion (Table 2, compare entries 1 and 4). In contrast to the reaction with **2**, diol predominated among the oxidation products and the yield of its overoxidation product, ketol, also increased. As in the **2**-catalyzed process, the reaction in the presence of **1** was greatly accelerated by the addition of acid (entry 5 in Table 2; Figure 1b), which also led to an improvement in the H_2O_2 utilization efficiency. In contrast to the **2**-catalyzed reaction, CyH oxidation in the presence of **1** could successfully proceed with 0.1 *M* H_2O_2 (Table S2). The use of more concentrated H_2O_2 reactant (50% instead of 30% aqueous solution) produced only a minor effect on the maximum achievable CyH conversion and epoxide selectivity (Table S2). An isolated peroxo species, **6**, could be also used as the catalyst (Table 2, entry 11).

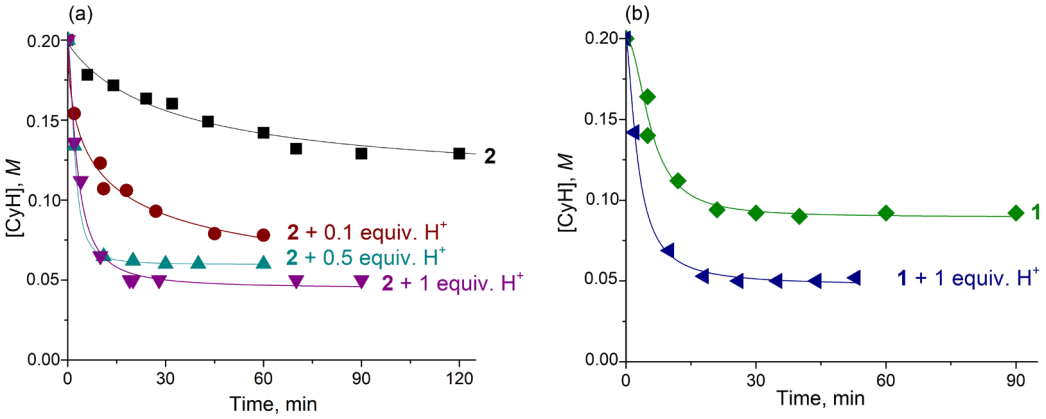

Figure 1. Effect of acid on CyH oxidation rate in the presence of (a) **2** and (b) **1** (0.004 *M* Zr, 0.2 *M* CyH, 0.2 *M* H_2O_2 (30%), 0.0004-0.004 *M* $HClO_4$ (if any), 1 mL CH_3CN, 50 °C).

Stability of the Lindqvist Zr-POM under the turnover conditions of the CyH oxidation was verified using FT-IR spectroscopy. The IR spectrum of the catalyst recovered from the reaction mixture by precipitation with ether revealed all the main vibrations of the Lindqvist structure (Figure S4). Disappearance of the characteristic feature at 731 cm^{-1} attributed to Zr-O(H)-Zr vibrations indicated that **2** was converted to a monomeric $\{ZrW_5\}$ species during the catalytic process and the

increase in terminal ν(W=O) suggests the presence of a more electronegative ligand at Zr, which is consistent with peroxide.

The catalytic performances of **2** and **1** were then tested in the epoxidation of various alkenes with aqueous H_2O_2 (Table S3). For cyclooctene (CyOct), selectivity towards the corresponding epoxide reached 96−100%, the monomer being more active and selective. Styrene produced, along with epoxides, a significant amount of benzaldehyde, the product of the oxidative C=C bond cleavage. In the oxidation of methyl oleate and *cis*-stilbene, predominantly *cis*-epoxides were formed, indicating a concerted mechanism of oxygen atom transfer that involves no radical or ionic intermediate capable of rotation around the C−C bond.

Catalytic Performance of Zr-POMs in Oxidation of α, β-Unsaturated Carbonyl Compounds. The Lindqvist Zr-POMs revealed pronounced activity for the epoxidation of electron-deficient C=C bonds in α,β-unsaturated carbonyl compounds (Table 3). The oxidation of carvone resulted in the predominant formation of 7,8-epoxide rather than 1,2-epoxide (ca. 10:1), i.e. oxidation of the more nucleophilic C=C bond. Such specific regioselectivity in the carvone epoxidation coupled with the high heterolytic pathway selectivity found for CyH oxidation (Table 2) indicates the formation of electrophilic oxidizing species. Importantly, the **2**-catalyzed carvone oxidation proceeded easily not only in acetonitrile solvent, but also in ethyl acetate (Table 3), which implies that the active oxidant is a zirconium peroxo species rather than peroxyimidic acid that might be formed upon interaction of CH_3CN and H_2O_2 (the so-called Payne oxidation).

Table 3. Oxidation of α,β-Unsaturated Compounds with H_2O_2 in the Presence of Zr-POMs[a]

Substrate	Catalyst	Time,[b] h	Substrate conv., %	Epoxide selectivity, %
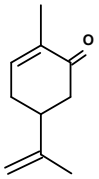	**2**	0.3	65 (68)[c]	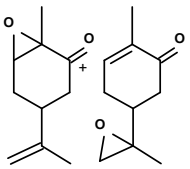 51[d] (47)[c,d]
	1	0.3	43	54[d]
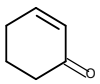	**2**	0.7	80	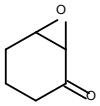 48[e]
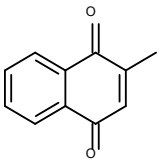	**2**	1	23	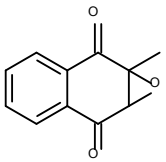 87

[a]Reaction conditions: 0.1 *M* substrate, 0.8 *M* H_2O_2, 0.002 *M* Zr, CH_3CN 1 ml, 70°C. [b]Optimal reaction time to reach the maximum selectivity and conversion. [c]Ethyl acetate was used as solvent instead of CH_3CN. [d]7,8-epoxide to 1,2-epoxide ratio was ca. 10 : 1; other products: hydroxycarvone, isomers of diepoxycarvone and epoxycarvonediol. [e]Other products: 4-hydroxy-2-cyclohexen-1-one, 2,3-dihydroxycyclohexanone, 4-acetylbutyric acid.

Catalytic Performance of Zr-POMs in Oxidation of S-Compounds. The oxidation of methyl phenyl sulfide (MPS) with 1 equiv. of H_2O_2 in the presence of **1** and **2** as catalysts produced the corresponding sulfoxide as the main product with 89 and 77% selectivity, respectively, at 81–82% substrate conversion (Table 4). The reaction was completed within 0.5 h at nearly room temperature and the oxidant utilization efficiency was as high as 91–99%. The excellent selectivity based on the oxidant implies that unproductive decomposition of H_2O_2 was negligible during the reaction course. In contrast to the oxidation of CyH, (i) the effect of the Bu_4NOH additive on the reaction selectivity was minor and (ii) Zr-free Lindquist tungstate $\mathbf{W_6}$ exhibited some activity in MPS oxidation, however much lower than that of $\{ZrW_5\}$-species (Table 4). Predomination of sulfoxide among the oxidation products indicates the formation of electrophilic oxidizing species upon interaction of Zr-

POM and H_2O_2. This contrasts drastically with thioether oxidation over Zr-MOFs, for which sulfone was the predominated product (99% selectivity at 49% MPS conversion).[57,58]

Table 4. MPS Oxidation with H_2O_2 in the Presence of Zr-POMs[a]

Catalyst	Time, h	MPS conv., %	H_2O_2 eff.,[b] %	Product selectivity,[c] %	
				MPSO	$MPSO_2$
-	24	14	17	79	21
2	0.5	82	91	89	11
2 + OH^{-}[d]	1.5	78	90	85	15
1	0.5	81	99	77	23
$\mathbf{W_6}$	5	26	28	92	8

[a]Reaction conditions: 0.1 *M* MPS, 0.1 *M* H_2O_2, 0.002 *M* Zr, 27 °C, CH_3CN 1 mL. [b]H_2O_2 utilization efficiency = total yield of products based on the oxidant consumed. [c]Based on substrate consumed. [d]0.002 M Bu_4NOH.

This suggestion was further confirmed by oxidation of the well-known test substrate thianthrene-5-oxide (SSO), the molecule of which possesses both nucleophilic and electrophilic sulfur (Scheme S1). The ratio of thianthrene 5,5-dioxide (SSO_2) and 5,5,10-trioxide ($SOSO_2$, product of further oxidation of both oxides) to all products, including, thianthrene 5,10-dioxide (SOSO) gives the so-called nucleophilic parameter X_{Nu} ($X_{Nu} = (SSO_2 + SOSO_2)/(SOSO + SSO_2 + 2SOSO_2)$). The value of $X_{Nu} \leq 0.3$ specifies electrophilic character of oxidant, while $X_{Nu} \geq 0.7$ indicates nucleophilic oxidation.[100] H_2O_2-based oxidation of SSO in the presence of **2** gave the value of X_{Nu} equal to 0.25. Note that, in the SSO oxidation over UiO-66, this parameter was found to be 0.92 and supported the proposed nucleophilic oxidation mechanism in the presence of Zr-MOF.[57]

Finally, the competitive oxidation of *p*-Br-methyl phenyl sulfide and methyl phenyl sulfoxide with H_2O_2 showed a higher yield of *p*-Br-methyl phenyl sulfoxide (11%) with respect to methyl phenyl sulfone (1%), which also points to the electrophilic nature of the oxidant.[101] Again, this

contrasts drastically with the catalytic performance of UiO-66 for which the ratio of methyl phenyl sulfone to *p*-Br-methyl phenyl sulfoxide was recently estimated as 24.[57]

Collectively, these results allowed us to conclude that, in contrast to Zr-MOFs which realize predominantly nucleophilic activation of hydrogen peroxide,[57] electrophilic activation takes place when the catalyst is the Lindqvist Zr-POM.

Kinetic Studies in the Alkene Oxidation by Zr-POM. To shed more light on the oxidation mechanism over Lindqvist Zr-POM, the kinetics of CyOct oxidation with H_2O_2 in the presence of **2** were studied. CyOct was chosen as a model substrate due to its lower volatility than CyH, its more stable epoxide and its superior epoxidation selectivity based on both substrate and oxidant. The kinetic curves for CyOct decay and epoxide product accumulation showed no induction period, autocatalysis or inhibition behavior. The absence of the effect of light, molecular oxygen or common chain radical scavengers, e.g., ionol, on the reaction rate precluded a radical chain oxidation mechanism, which is consistent with the minor amount of the allylic oxidation products formed in the oxidation of CyH.

The rate of CyOct oxidation in the presence of **2** exhibited a typical Arrhenius dependence (Figure 2), which implies that there was no change in the rate-limiting step over the assessed temperature range. The value of the apparent activation energy (10.3 kcal mol^{-1}) turned out to be lower than those previously found for TiW_5- and NbW_5-catalyzed CyOct epoxidation (14.3 and 11.7 kcal mol^{-1}, respectively).[93]

The reaction orders in the alkene substrate and H_2O_2 were fractional (< 1) and had a tendency to decrease with increases in their concentration (Figure S5, (a) and (b), respectively), which may indicate comparable rates for the formation of an active peroxo intermediate and subsequent oxygen transfer to the substrate.[57] The reaction order in **2** was found to be close to 0.5 (Figure S5c). This can be rationalized if we suggest that the formation of the active peroxo species involves dissociation of

the dimer, which is relatively slow. A similar trend was observed earlier for H_2O_2-based thioether oxidation catalyzed by the Ti-monosubstituted μ-hydroxo Keggin type dimer $[Bu_4N]_7[(PTiW_{11}O_{39})_2OH]$[102] and cyclooctene epoxidation with the Nb-monosubstituted μ-oxo Lindqvist dimer $(Bu_4N)_4[(NbW_5O_{18})_2O]$.[92] Finally, the rate of CyOct oxidation revealed almost no dependence on the concentration of water (Figure S5(d)).

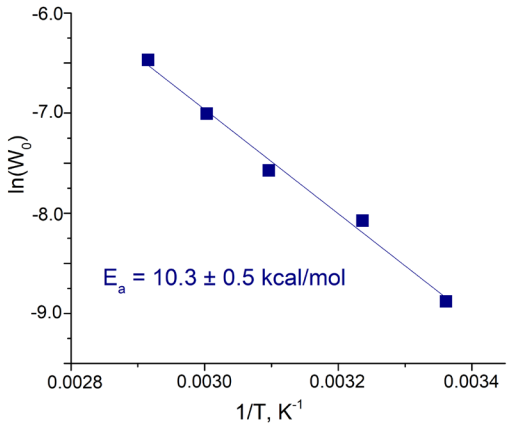

Figure 2. Dependence of the initial rate (W_0) of **2**-catalyzed CyOct epoxidation on the reaction temperature in Arrhenius coordinates (CyOct 0.1 M, H_2O_2 0.1 M, **2** 0.002 M).

Interaction of Zr-POMs with H_2O_2: Spectroscopic Characterization of Reaction Intermediates. To probe the formation of active peroxo zirconium species, the interaction of dimer **2** and monomer **1** with hydrogen peroxide was investigated using UV-vis spectroscopy. The UV-vis spectra of initial **1** and **2** are given in Figure S3. A gradual addition of H_2O_2 to **2** caused a hypsochromic shift of the UV absorption band along with an increase in the intensity (Figure 3). Kortz and co-workers observed absorption in the same UV region for Zr^{IV} peroxide $[Zr_2(O_2)_2(\alpha\text{-}SiW_{11}O_{39})_2]^{12-}$.[103] They also reported a decrease in its intensity and a slight bathochromic shift upon interaction with methionine.

The reaction between H_2O_2 and **2** was very fast, the spectral changes occurred immediately after the H_2O_2 addition and no subsequent change was observed. Importantly, it was not possible to

attain equilibrium because the optical density continued steadily to increase with the addition of a new portion of 30% H_2O_2 (Figure 3). This might suggest co-existence of two or more processes in the presence of a large excess of aqueous H_2O_2. With 77% H_2O_2, the system was closer to equilibrium (Figure S6), indicating that the presence of water is crucial for these processes. On the other hand, the addition of water (up to 5 vol.%) to a solution of **2** produced negligible changes in the UV-vis spectrum (Figure S7), which implies that hydrolysis of the Lindqvist Zr-POM dimer is a rather slow process, at least, at room temperature (or thermodynamically unfavorable). Indeed, Errington et al. reported earlier that only the hydroxy derivative **2** and no monomer **1** were detected after interaction of the methoxy dimer **2'** with 200 equiv. (8 vol%) of H_2O for 30 min at 60 ^oC (or alternatively, 38 equiv. (1 vol%) for 67 h at 70-80 ^oC).[104]. The changes in the UV spectra of **1** after the addition of H_2O_2 revealed a trend similar to that acquired for **2** and involved a hypsochromic shift of the absorption band along with steadily increasing intensity (Figure S8).

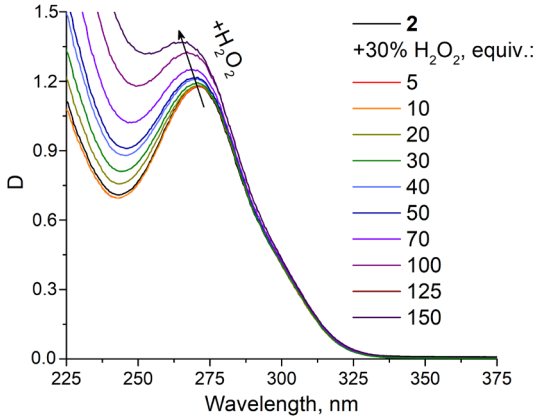

Figure 3. UV spectral changes of **2** upon addition of 30% H_2O_2 (5÷150 equiv. to Zr). Conditions: 0.25 m*M* **2**, 2.5÷75 m*M* H_2O_2, dry CH_3CN, 20 ^oC, l = 0.2 cm.

The methoxido derivative of **2**, dimer **2'**, enriched with ^{17}O was employed to study the interaction between Zr-POM and H_2O_2 by means of ^{17}O NMR spectroscopy. The use of **2'** was justified by the fact that the catalytic performance of **2'** was very similar to that of **2** (see Table 2).

After the addition of small amounts of anhydrous H_2O_2 (0.5-5 equiv.) to the solution of **2'**, a downfield shift could be observed for the signals of W=O (719 and 700 ppm vs 714 and 694 ppm in **2'**) and μ_6O (-45 vs -56 ppm) (Figure 4, spectra C and D). The signal attributed to Zr-O-W underwent a noticeable upfield shift (475 vs 487 ppm in **2'**), while the position of the W-O-W signal (δ 388 ppm) remained unchanged (Figure 4, C and D). If a smaller amount of H_2O_2 (0.25 equiv. per Zr) was added, one could observe two separate ^{17}O NMR signals for both W=O, Zr-O-W and μ_6O oxygens (Figure 4, spectrum B), indicating the appearance of a new form of the Zr-POM. When 0.5 equiv. of H_2O_2 was added, the signals of **2'** disappeared completely, indicating that transformation between the two forms is complete. It should be noted that no hydrolysis of **2'** occurred during the interaction of **2'** with H_2O_2, as peaks characteristic of **2** (Zr-O-W signal at δ 487 ppm) were not present (see Figure S9), which is reasonable, given that **2'** is not very readily hydrolyzed,[104] and that H_2O_2 was used as an anhydrous solution in acetonitrile. The difference between the ^{17}O NMR spectra of **2** and **2'** + H_2O_2 is clearly manifested by the position of the signals of W=O and μ_6O. Starting from 5 equiv. of H_2O_2 some broadening of the ^{17}O NMR signals could be observed (Figure 4, spectrum D). Importantly, the spectrum of the mixture did not change after prolonged storage at room temperature, which indicates that the mixture is equilibrated.

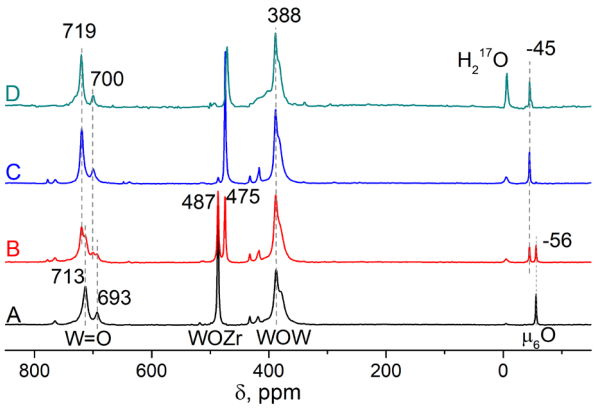

Figure 4. ^{17}O NMR spectra of (A) **2'**, (B)-(D): **2'** reacted with 0.25, 0.5, and 5 equiv. (per Zr) of H_2O_2 (**2'** 0.03 *M*, dry CH_3CN, 20 °C).

^{183}W NMR spectroscopy was employed to study interaction of dimer **2** with aqueous H_2O_2 (Figure 5). After the addition of 0.5 equiv. of H_2O_2, a couple of two new signals (δ 60.1 and 44.7 ppm) appeared in the ^{183}W NMR spectrum in addition to the signals of initial **2** and can be therefore attributed to the formation of a peroxo species. The intensity ratio of ca. 1:4 indicates that the peroxo species also has a structure of the monosubstituted Lindqvist anion. Some upfield shifting of the signals of initial **2** (74.1 vs 78.2 ppm and 49.3 vs 50.8 ppm) could be due to the presence of water in the acetonitrile solution (added with H_2O_2), as was confirmed by an independent experiment with water additives (see Figure 5, spectrum D). The subsequent addition of 1 equiv. of MPS caused disappearance of the signals at δ 60.1 and 44.7 ppm supporting their attribution to the active peroxo species (Figure 5, spectrum C). Further addition of H_2O_2 caused an extra signal shifting and broadening of the signals attributed to the peroxo species (Figure S10). These changes are consistent with those observed in the ^{17}O NMR spectra (Figure 4) and suggest subsequent transformations of the peroxo species upon increasing concentration of H_2O_2.

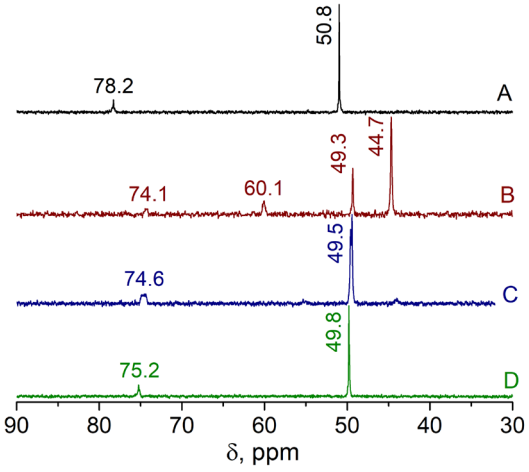

Figure 5. ^{183}W NMR spectra of **2** (0.045 *M* in CD_3CN, 20°C, curve A), **2** after interaction with 0.5 equiv. (per Zr) of H_2O_2 (curve B) followed by the addition of 1 equiv. of MPS (curve C), **2** after addition of 13 μL of H_2O (curve D).

The interaction between **2** and hydrogen peroxide was also investigated by *in situ* IR spectroscopy. The addition of H_2O_2 resulted in the disappearance of the 735 cm^{-1} feature attributed to Zr-O(H)-Zr and appearance of a new band at 791 cm^{-1} (Figure 6a) that can be assigned to the wagging of ZrO_4 moieties, active after symmetry breaking (see discussion of simulated spectra, below). Importantly, this band disappeared after the addition of methyl phenyl sulfide while the band at 735 cm^{-1} completely restored, indicating return to the initial dimer **2** (Figure 6b). GC analysis of the reaction mixture showed 96% conversion of MPS along with 86% yield of MPSO and 10% yield of $MPSO_2$.

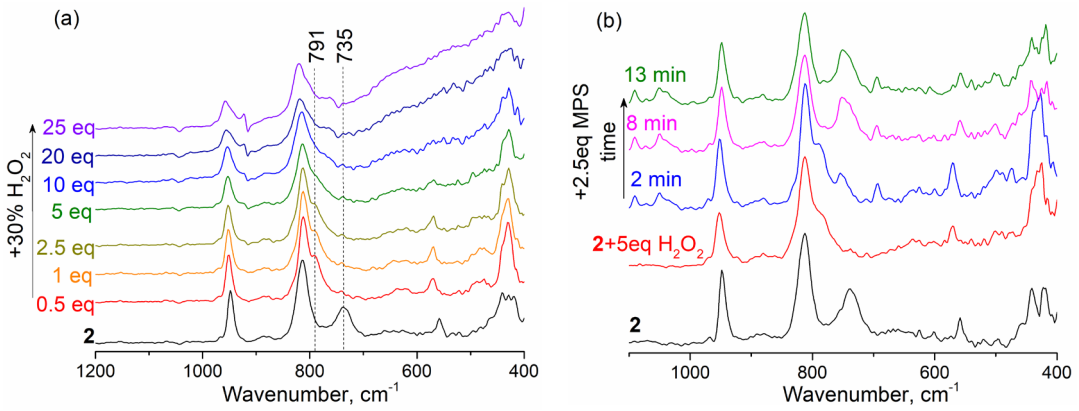

Figure 6. Changes in the IR spectrum of **2** (0.01 *M*) in CH_3CN (0.5 mL) at room temperature after (a) addition of 0.5 - 25 equiv. (per Zr) of H_2O_2 and (b) after addition of 5 equiv. (per Zr, 0.1 *M*) of H_2O_2 followed by the addition of methyl phenyl sulfide (0.05 *M*). The spectrum of CH_3CN was subtracted.

To shed some light onto the structure of the Zr-peroxo species formed by the interaction of **2** with H_2O_2, we performed DFT calculations;[105,106] and initially we evaluated the relative stability of several possible species (Scheme 2). The characterized structures lie in a very narrow range of energies (Scheme 2), in line with the experimental observations that point towards the formation of a mixture of peroxo-containing species in equilibrium. The most stable dimeric peroxo complex is $[(\mu\text{-}\eta^2\text{:}\eta^2\text{-}O_2)\{ZrW_5O_{18}\}_2]^{6-}$ (shown in Figure S11), being only 0.5 kcal mol^{-1} above **2** in terms of free

energy. This species is followed in stability by two monomeric complexes, the Zr-hydroperoxo $[W_5O_{18}Zr(\eta^2\text{-}OOH)]^{3-}$ and the Zr-peroxo $[HW_5O_{18}Zr(\eta^2\text{-}OO)]^{3-}$ protonated at a bridging Zr-O-W site (Figure S11), which are only 0.8 and 1.0 kcal mol^{-1} less stable than their dimeric partner, indicating that indeed, the equilibria between these species should be sensitive to the concentration of oxidant. Dimeric structures in which both bridging ligands contain peroxo or hydroperoxo units were computed to be less stable, being above in energy than **2** by 6.9 and 9.8 kcal mol^{-1}, respectively.

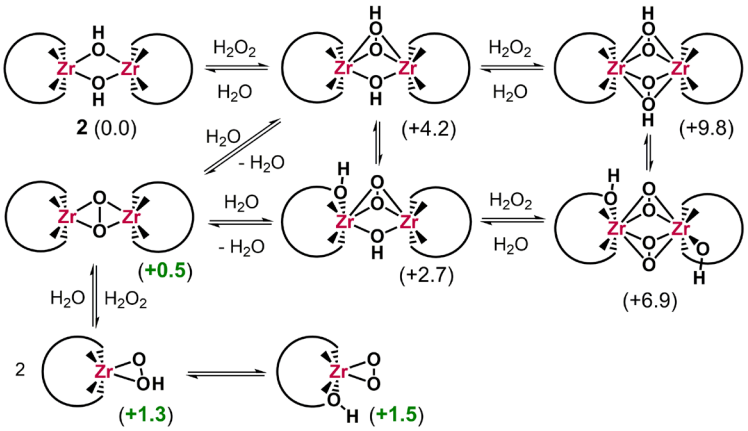

Scheme 2. DFT study of the possible species formed upon the interaction of **2** with aqueous H_2O_2 that would correspond to species **3**-**11**. Relative Gibbs free energies in kcal mol^{-1}.

Notably, the DFT-simulated IR spectra of the species in Scheme 2, shown in Figure 7, can nicely reproduce the variations observed experimentally upon treating **2** with H_2O_2 (Figure 6a). First, the feature at 742 cm^{-1} (experimentally at 735 cm^{-1}), associated to the bending of the μ-OH protons (Figure S12) disappears in the peroxo complexes; whereas a new band appears at 772 cm^{-1} (experimentally at 791), associated to the wagging of Zr-bound oxo ligands of the ZrO_4 moiety, as shown in Figures S13 and S14. Note that in going from the dihydroxo dimer **2** to the peroxo dimer, one of the POM subunits flaps out of the $\{Zr(\eta^2\text{-}O_2)\}$ plane, resulting in a change of the symmetry that makes the band associated to the wagging of ZrO_4 active (see Figure S12 and S13). Also along the series, simulated spectra show shifts to higher energies of the bands at 967 and 793 cm^{-1}, which

can be also appreciated in Figure 6a. This trend can be ascribed to global charge effects that reduce the negative charge of the tungstate framework and yield more compact structures with shorter W-O bond distances. Finally, the new band that appears for the monomeric Zr-(η^2-OO) at 748 cm^{-1} (Zr-oxo wagging shifted down by the effect of protonation, Figure S14) could be related to the shoulder at ca. 760 cm^{-1} observed in the experimental spectra upon increasing the amount of H_2O_2 (Figure 6a).

Comentario [c1]: Here I eliminated a duplicate sentence

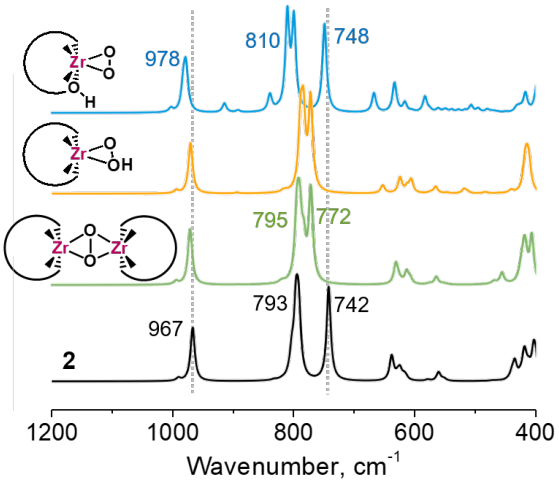

Figure 7. Comparison of the DFT-simulated IR spectra for compound **2** and the most stable Zr-peroxo species.

The spectroscopic analysis (UV-vis, ^{17}O NMR, IR and Raman) was extended to a series of solids prepared by the addition of different amounts of H_2O_2 to complexes **2** and **1** (see Table 1 for details). These results, as well as the use of combined HPLC-ICP-AES technique, collectively support the formation of dimeric and monomeric peroxo Zr complexes, as described above (see Figures S16–S23, and corresponding discussion in the Supporting Information). We also employed the HR-ESI-MS technique to characterize the peroxo species formed upon interaction of dimer **2** and H_2O_2 (see Figures S24–S28, and corresponding discussion in the Supporting Information). The HR-ESI-MS spectra showed peaks corresponding to dimeric peroxo anion $(Bu_4N)_xH_y[\{W_5O_{18}Zr\}_2(\mu$-

η^2:η^2-O_2)]$^{6-x-y}$ (x = 0–4, y = 0–4) (Figure S24) and, most likely, monomeric zirconium superoxo species [{$W_5O_{18}Zr$}(OOH)]$^{2-}$ and [Bu_4N{$W_5O_{18}Zr$}(O_2)]$^{2-}$ which might derive from the corresponding hydroperoxo [{$W_5O_{18}Zr$}(OOH)]$^{3-}$ and peroxo [Bu_4N{$W_5O_{18}Zr$}(O_2)]$^{3-}$, respectively, under the conditions of the HR-ESI-MS measurements (Figure S25). Interestingly, these three anions are analogous to computed, lowest-energy, peroxo species resulting from the reaction of dimer **2** with H_2O_2 (Scheme 2). So far, attempts to grow X-ray quality crystals of the peroxo Zr species formed in the excess of H_2O_2 failed, most likely because of the high lability of Zr(IV) terminal ligands.[107] The product from the reaction between **2'** and 1 equiv. of H_2O_2 (per Zr) was apparently unstable, and crystals obtained by crystallization at -20 °C were shown to be **2** by a single-crystal X-ray diffraction study.

Reactivity of Zr-peroxo Species. We also investigated the stoichiometric interaction of the isolated peroxo species **3**–**11** with CyH and MPS as model substrates of different nucleophilicity. Scheme 2 provides tentative structures for these peroxo species derived from DFT calculations. Tables 5, S5, and S6 collect the results for CyH and MPS substrates, respectively. Peroxo species **3** and **4** obtained using 5 and 10 equiv. of H_2O_2 per Zr were completely inactive in CyH oxidation, while both **1** and **2**-derived peroxo species (compounds **8** and **5**) obtained using 20 equiv. of H_2O_2 revealed some activity toward CyH (Table 5). Compounds **6**, **7**, and **9** prepared with 35–50 equiv. of H_2O_2 were able to oxidize CyH under stoichiometric conditions, leading to epoxide and diol with a fairly good carbon and oxygen mass balance under the assumption that one active oxygen is present in the peroxo species (Table 5). **2**-Derived peroxo species **10** and **11** obtained using 35 equiv. of 50 or 77% H_2O_2 revealed CyH oxidation activity similar to that of **6** and **1**-derived **9**. The addition of Bu_4NOH in the amount of 1 equiv. to Zr resulted in deactivation of the peroxo species, while 1 equiv. of acid favored further oxidation of CyH and formation of ketol (Table 5). Interestingly, the addition of one more equivalent of protons did not stimulate further oxidation.

Table 5. Stoichiometric Oxidation of CyH with Isolated Zr-peroxo Species

Peroxo species	CyH conv., %	TOF, min^{-1}	Product yield, %		
			Epoxide	Diol	Ketol
3	No reaction				
3 +1 equiv. H^{+a}	No reaction				
4	No reaction				
4+1 equiv. H^{+a}	11	0.01	3	3	2
5	9	0.02	6	2	-
5 + 1 equiv. H^{+a}	25	0.03	6	11	8
6	20.5	0.07	16	4	-
6 + 1 equiv. H^{+a}	34	n.d.	4.5	20	9
6 + 2 equiv. H^{+b}	33	n.d.	6	20	7
6 + 1 equiv. OH^{-c}	5	0.005	1	2.5	-
7	20.5	0.07	17.5	2.5	-
8[d]	12	0.03	6.5	5	-
9[d]	20	0.08	15	5	-
10	20	0.07	17	3	-
11	21	0.07	16	5	-

Reaction conditions: 0.016 *M* Zr, 0.08 *M* CyH, CH_3CN 1 mL, 26 ^oC, 1 h.
[a] 0.016 *M* $HClO_4$. [b] 0.032 *M* $HClO_4$. [c] 0.016 *M* Bu_4NOH (enol 1% was also formed). [d] Prepared from monomer **1** while other peroxo species derived from dimer **2**.

All peroxo derivatives **3**-**11** revealed activity in the oxidation of the thioether MPS (Table S5). Moreover, the yields of the oxidized products, sulfoxide and sulfone, increased significantly with the increasing amount of H_2O_2 used in the synthesis of the peroxo species, indicating a growing amount of active peroxo groups (Tables S5 and S6). As discussed above, increasing the amount of H_2O_2 favors the generation of monomeric (hydro)peroxo species, in which the number of active peroxo moieties per Zr atom is larger than for the low-energy peroxo dimers (see Scheme 2). Yet, we cannot completely exclude that such compounds possibly comprise peroxo groups coordinated not

only to Zr(IV) but also to W(VI). If so, these tungsten peroxo species are very weak because no changes in the ^{17}O NMR spectra could be observed upon addition of H_2O_2 to W_6.

In the next section, we will also show that computed barriers for oxygen transfer from monomeric species are lower in energy than from dimeric structures, explaining the trends observed in the oxidation of CyH substrate: the larger amount of H_2O_2 is used in the synthesis, the larger proportion of monomeric species are obtained, and the more oxidation activity is observed (Tables 5 and S6).

DFT Characterization of the Reaction Mechanism. Next, we conducted DFT calculations in order to provide an atomistic description of the reaction mechanism. Figure 8 shows the calculated Gibbs free energy profile for the epoxidation of CyH catalyzed by the Zr-hydroxido species $[W_5O_{18}Zr(OH)]^{3-}$, namely **A**, which corresponds to the active form of the catalyst that is regenerated after the oxygen transfer to the substrate from the monomeric hydroperoxo species represented in Scheme 1. As calculations will show (see discussion below), and in line with the interpretation of experimental results, the monomeric (hydro)peroxo species are significantly more reactive than the corresponding dimeric ones. Also, it is worth noting that although the assembly of two monomeric hydroxido complexes **A** to form dimer **2** is slightly exergonic (by 2.7 kcal mol^{-1}), under catalytic conditions, the dimerization of **A** is less likely than the reaction with H_2O_2 and the substrate, which are at much higher concentrations. Therefore, the dimer **2** should act as a catalyst precursor, and its formation in significant amounts is unlikely during the turnovers. We also want to point out that in water solvent, complex **A** might spontaneously coordinate a water molecule to generate a $[W_5O_{18}Zr(OH)(OH_2)]^{3-}$ species,[107-109] although this process was computed to be slightly endergonic in acetonitrile (ΔG = +1.7 kcal·mol^{-1}). Thus, as illustrated in Figure 8, the catalytic process can initiate by the coordination of a H_2O_2 molecule to **A** forming the adduct **A-HP** (ΔG = -1.0 kcal mol^{-1}), in which one oxygen atom of the oxidant is incorporated to the labile coordination sphere of

Zr(IV). Then, the heterolytic activation of H_2O_2 proceeds through a rapid proton transfer from the oxidant to the hydroxido ligand involving **TS-1** ($\Delta G^{\ddagger}$ = 6.9 kcal mol^{-1}), which can be accelerated by the assistance of a water molecule acting as a proton shuttle. This latter pathway proceeds through transition state **TS-1$_w$** and has a very low free-energy barrier of 3.7 kcal mol^{-1}. The computed geometries for **TS-1** and **TS-1$_w$** are represented in Figure S29. The overall formation of Zr-hydroperoxo complex **B** from **A** is exergonic by 1.4 kcal mol^{-1}. Complex **B** can coexist in equilibrium with the Zr-peroxo complex **C** protonated at a Zr-O-W bridging site of the POM because the computed energy difference is only 0.2 kcal mol^{-1} (see Figure 8) and there is a smooth free-energy barrier connecting **B** and **C**, 13.5 and 5.7 kcal mol^{-1} for non- and water-assisted mechanisms, respectively (see Figure S30 for the corresponding transition state structures).

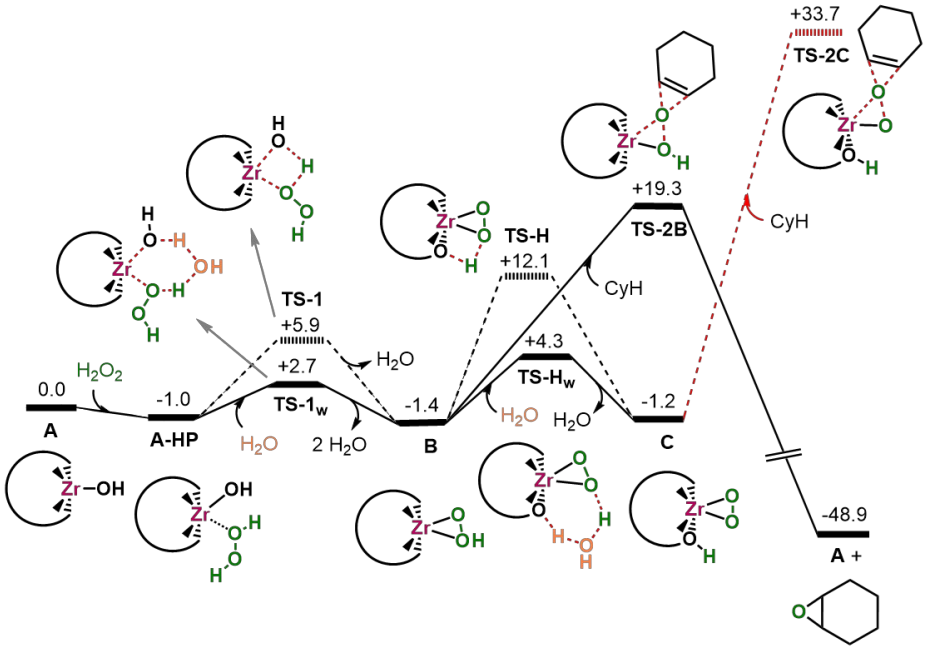

Figure 8. Gibbs free-energy profile (kcal mol^{-1}) for the epoxidation of CyH with H_2O_2 catalyzed by **A**. Black solid lines correspond to the minimum-energy reaction pathway, whereas dashed lines are associated to more energetic mechanisms.

As shown in Figure 8, the oxygen transfer to the double bond of the alkene can be attained more easily from the Zr-hydroperoxo **B** through transition state **TS-2B** (Figure 9a) with a moderate free-energy barrier (20.7 kcal mol^{-1}), whereas a prohibitively high barrier of 34.9 kcal mol^{-1} is computed for the transfer from Zr-peroxo species **C** through transition state **TS-2C** (Figure 9b). This process readily yields the epoxide product irreversibly and regenerates the active form of the catalyst (**A**). Thus, the monomeric Zr-hydroperoxo **B** was identified as the active epoxidizing species and the hydroperoxo α-oxygen transfer as the rate-determining step. In line with the interpretation of experimental results, the computed free-energy barriers for the O-transfer to CyH from dimeric peroxo $[(\mu\text{-}\eta^2\text{:}\eta^2\text{-}O_2)\{ZrW_5O_{18}\}_2]^{6-}$ (**D**) and hydroperoxo $[(\mu\text{-}\eta^2\text{:}\eta^2\text{-}OOH)(\mu\text{-}OH)\{ZrW_5O_{18}\}_2]^{6-}$ complexes are significantly higher in energy (29.6 and 28.9 kcal mol^{-1}, respectively; and Figures 9c and S31 for transition state structures). Interestingly, in the latter case the β-oxygen transfer from the Zr bridging hydroperoxo becomes very close in energy to the α-oxygen one (< 1 kcal mol^{-1}; see Figure S31), indicating that Zr-hydroperoxo moiety is in a hindered environment.[110] In fact, we have shown that the steric repulsion between the alkene substrate and the POM framework can influence the activity of epoxidation reactions.[111] Accordantly, the computed barriers for the oxygen transfer to the more reactive and less sterically demanding MPS substrate[112] from monomeric hydroperoxo complex **B** and dimeric peroxo complex **D** (18.5 and 22.3 kcal mol^{-1}, respectively) are lower than for CyH substrate and closer to each other (Figure S33). Moreover, the barrier for the dimeric structure becomes accessible at the reaction conditions, explaining why experimentally this species does not react with alkenes but it does with thioethers. Figure 10 shows a summary of the mechanistic proposal for the different substrates.

To further validate the proposed mechanism, we compared the DFT results with the experimental Arrhenius activation energy (E_a) for the epoxidation of CyOct. In the absence of thermal and entropic effects, the rate-determining step (**B** → **TS-2B**) has a zero-point-corrected energy barrier of 9.5 kcal mol^{-1} for the epoxidation of CyOct (10.0 kcal mol^{-1} for epoxidation of

CyH), which is very close to the experimental E_a value of 10.3 kcal mol^{-1}. Additional calculations on the α-oxygen transfer to carvone substrate by Zr-hydroperoxo complex **B** also support the electrophilic nature of the proposed epoxidizing species. Thus, the computed free-energy barrier for the α-oxygen transfer to the more nucleophilic 7,8 double bond ($E(\pi_{C=C})$ = -7.05 eV) was 24.2 kcal mol^{-1}, 2.3 kcal mol^{-1} lower than that to the less nucleophilic 1,2 bond ($E(\pi_{C=C})$ = -7.23 eV). The difference between these free-energy barriers is in qualitative, if not quantitative, agreement with the experimental product distribution (Table 3).

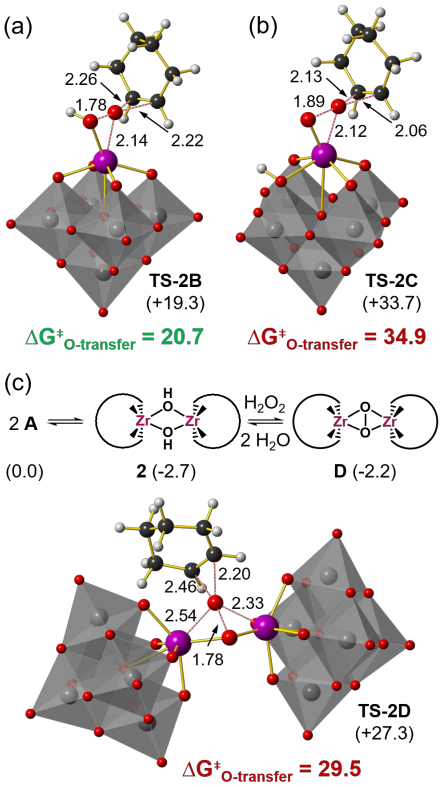

Figure 9. Optimized geometries of the transition states for the oxygen-transfer to CyH by monomeric hydroperoxo species, **TS-2B** (a), monomeric peroxo, **TS-2C** (b), and dimeric peroxo, **TS-2D** (c). Free-energy barriers, and relative free-energies respect to compound **A** (in parenthesis) are given in kcal mol^{-1}. Main distances are shown in Å.

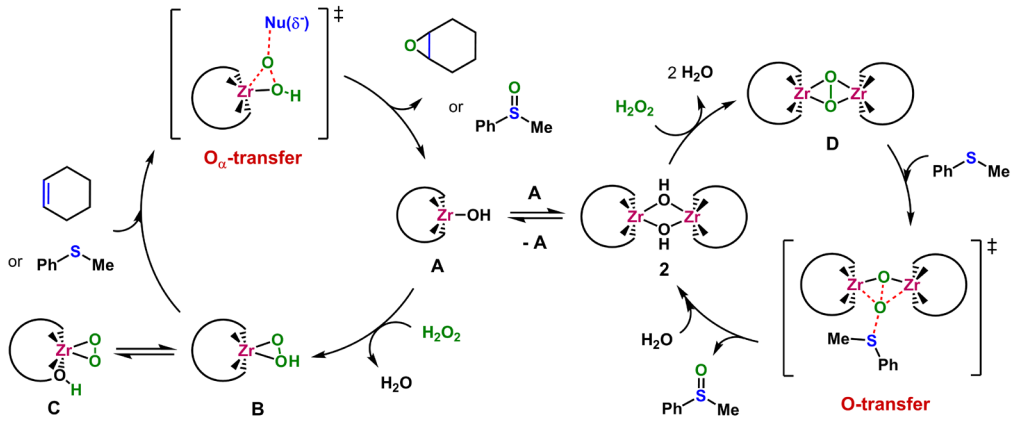

Figure 10. Schematic summary of the key mechanistic findings for the oxidation of organic substrates with H_2O_2 catalyzed by Zr-monosubstituted Lindqvist tungstates.

We next investigated how the presence of acid additives affect the reaction mechanism and accelerate the reaction kinetics (compare entries 1 and 4 with 2 and 5 in Table 2). Previous studies with Ti and Nb POMs already showed that the protonation of the catalyst (decreasing its formal negative charge) results in a higher electrophilic character of the TM-(hydro)peroxo group and therefore, decreases the energy barrier for the O-transfer step.[92,99] For Zr-hydroperoxo species we find an analogous situation (Figure S34). Upon protonation, we found that the free-energy barrier for the O-transfer step is reduced from 20.5 to 17.7 kcal mol^{-1}. The protonation of dimeric peroxo $[(\mu\text{-}\eta^2\text{:}\eta^2\text{-}O_2)\{ZrW_5O_{18}\}_2]^{6-}$ (**D**) complex also reduces the computed free-energy barriers for the O-transfer to CyH by 3.7 kcal·mol^{-1}. However, the resulting barrier of 25.8 kcal·mol^{-1} would still be higher than that of the monomer (20.5 kcal·mol^{-1}). Moreover, under acidic conditions the Zr-hydroxido complex **A** could evolve to a Zr-triaqua species $[W_5O_{18}Zr(OH_2)_3]^{2-}$,[107,109] which lies slightly below in energy than the protonated Zr-hydroperoxo $\mathbf{B_H}$ and may act as the resting state of the protonated catalyst. Nevertheless, the overall free-energy barrier computed from Zr-triaqua species (18.6 kcal mol^{-1}, see Figure S34) is still lower than that calculated for the non-protonated catalyst. Moreover, low pH may also help in displacing the dimer-monomer equilibrium towards the monomer due to the protonation of terminal hydroxido ligands, which are essential for the

dimerization process.[109] As discussed above, the monomeric forms of the catalyst regenerated after each catalytic cycle are unlikely to dimerize; however, we cannot discard some improvement of the activity by accelerating the dissociation of dimeric precatalyst via protonation. It is also worth to note that other authors have shown that the dimer/monomer equilibrium of POMs controls the generation of active species for other catalytic processes.[113]

Finally, we compare the results obtained here for the Lindqvist Zr(IV)-POM $[W_5O_{18}Zr(OH)(OH_2)]^{3-}$ with our previous calculations on analogous Ti(IV)- and Nb(V)-POMs,[92,93] in order to understand the effect of metal nature on catalytic activity. Experimentally, the apparent activation energies follow the order: Zr(IV) < Nb(V) < Ti(IV) (see above); and accordantly, the computed overall free-energy barriers are: 20.7, 26.3 and 29.8 kcal mol^{-1}, respectively. The trend in going from Nb(V) to Zr(IV) catalyst may seem surprising. Both metal centers have flexible coordination environment, which are able to accommodate distorted 6-coordinated transition states, but Nb has a higher oxidation state that enhances the electrophilicity of the metal-hydroperoxo moiety.[93] Indeed, if we compare the single step of oxygen transfer from metal-hydroperoxo species, the computed free-energy barrier for the Lindqvist Nb(V)-POM (17.6 kcal mol^{-1}) is lower than for the corresponding Zr(IV)-POM (20.7 kcal mol^{-1}). However, looking at the complete picture of the reaction mechanism unveils another complementary factor that enhances the catalytic activity of Zr-POMs. Unlike Ti(IV)- and Nb(V)-Lindqvist catalysts, which form highly stable HW_5TM-(η^2-OO) resting states that have to interconvert into less stable W_5TM-(η^2-OOH) species to react with alkenes, Zr(IV) prevents the peroxo species from being significantly more stable than the epoxidizing hydroperoxo species, resulting in a formal reduction of the overall free-energy barrier and in turn, in the acceleration of the reaction rate.

CONCLUSIONS

Zr(IV)-substituted Lindqvist-type polyoxotungstates, $(Bu_4N)_2[W_5O_{18}Zr(H_2O)_3]$ (**1**) and $(Bu_4N)_6[\{W_5O_{18}Zr(\mu\text{-}OH)\}_2]$ (**2**), were successfully applied as catalysts for the mechanistic understanding of selective oxidation reactions mediated by H_2O_2 via heterolytic mechanisms. The scope of the reaction spans from epoxidation of unfunctionalized alkenes and α,β-unsaturated ketones to the sulfoxidation of thioethers. The presence of catalytic amounts of acid accelerates the reaction rate and enhances its selectivity, reaching oxidant utilization efficiency up to >99%. A comprehensive study by means of a wide variety of experimental and computational techniques, allowed us to identify three main Zr-peroxo species that are formed in equilibrium upon treating **2** with H_2O_2: a [(μ-η^2:η^2-O_2) dimeric; and two monomeric complexes bearing terminal peroxo or hydroperoxo ligands. Kinetic studies indicate that the reaction mechanism involves an oxygen transfer from a monomeric complex to the substrate and determined an activation energy (10.3 kcal mol^{-1}) for the epoxidation of CyOct that is lower than those reported previously for Nb(V)- and Ti(IV)-substituted Lindqvist catalysts.

DFT calculations on the reaction mechanism reproduce experimental trends and identify the monomeric Zr-hydroperoxo intermediate as the real epoxidizing species. The reaction proceeds through the heterolytic, α-oxygen transfer of Zr-hydroperoxo moiety to the nucleophilic C=C bond that was found to be the rate-determining step of the catalytic cycle, accounting for a free-energy barrier of 20.5 kcal mol^{-1}. The protonated form of the catalyst reduces its overall free-energy barrier by ca. 2 kcal mol^{-1}, as a result of the increase of the polyoxometalate electrophilic character, which explains the experimental trends upon acid addition. The higher reactivity of the monomeric form of the catalyst compared to the dimer was ascribed to the steric repulsions that hamper the approach of the alkene substrates to the electrophilic oxygens of the dimer. Also, the higher activity of Zr(IV)-based catalysts in comparison to Nb(V)- and Ti(IV)-substituted analogues was ascribed to two complementary factors: i) the high flexibility of the Zr coordination sphere that stabilizes the 7-fold coordinated transition state structure for the O-transfer step; and ii) the low tendency to form deep-

well, low-reactivity, Zr-peroxo intermediates due to the similar Brönsted basicity of the Zr-peroxo group and the Zr-O-W bridging sites. We hope that the understanding of the reaction mechanism and of the factors affecting the activity will not only serve to generate fundamental knowledge to this important catalytic process but to provide criteria for the design of novel catalysts.

AUTHOR INFORMATION

Corresponding Authors

* E-mails: khold@catalysis.ru; john.errington@newcastle.ac.uk; j.carbo@urv.cat

Author Contributions

The manuscript was written through contributions of all authors. / All authors have given approval to the final version of the manuscript.

Notes

The authors declare no competing financial interests.

ASSOCIATED CONTENT

Supporting Information. ^{183}W and ^{17}O NMR, FT-IR, Raman, UV-vis, and HR-ESI-MS spectra; HPLC-ICP-AES chromatograms; synthesis procedures; catalytic results; computational details; additional energy profiles; DFT-structures for relevant intermediates and transition states; and cartesian coordinates of computed structures.

ACKNOWLEDGMENTS

The authors thank Dr. I. E. Soshnikov, Dr. M. V. Shashkov, V. V. Volchek, and Dr. O. O. Zaikina for the ^{31}P NMR, GC-MS, HPLC-ICP-AES measurements, and CHN analysis, respectively. This work was partially supported by the Ministry of Science and Higher Education of the Russian Federation within the governmental order for the Boreskov Institute of Catalysis (BIC, project

AAAA-A21-121011390008-4), the Russian Foundation for Basic Research (grant 20-53-10008), and The Royal Society (grant IEC\R2\192205). The studies were carried out using facilities of the shared research center "National center of investigation of catalysts" at BIC and the Center of Collective Use «Mass spectrometric investigations». The Raman equipment was provided by REC «MDEST» NSU. J. J. C. and J.-M. P. thank the Spanish Ministry of Science (PGC2018-100780-B–I00 and CTQ2017-87269-P projects) for generous support. P. A. thanks the Ministry of Science and Higher Education of the Russian Federation (grant number 121031700313-8) for the access to analytical equipment.

REFERENCES

(1) *Modern Heterogeneous Oxidation Catalysis: Design, Reactions and Characterization*; Mizuno, N., Ed.; Wiley-VCH: Weinheim, 2009.

(2) *Liquid Phase Oxidation via Heterogeneous Catalysis: Organic Synthesis and Industrial Applications;* Clerici, M.G., Kholdeeva, O.A., Eds.; Wiley: Hoboken, 2013.

(3) *Handbook of Advanced Methods and Processes in Oxidation Catalysis;* Duprez, D., Cavani, F., Eds.; Imperial College Press: London, 2014.

(4) Cavani, F.; Teles, J. H. Sustainability in Catalytic Oxidation: An Alternative Approach or a Structural Evolution? *ChemSusChem* **2009**, *2*, 508–534.

(5) Jones, C.W. *Application of Hydrogen Peroxide and Derivatives*; Royal Society of Chemistry: Cambridge, 1999.

(6) Sheldon, R.; Arends, I. W. C. E.; Hanefeld, U. *Green Chemistry and Catalysis*; Wiley-VCH: Weinheim, 2007.

(7) Strukul, G., Scarso, A. In *Liquid Phase Oxidation via Heterogeneous Catalysis: Organic Synthesis and Industrial Applications*; Clerici, M. G., Kholdeeva O. A., Eds.; Wiley: Hoboken, 2013; p. 1.

(8) Campos-Martin, J. M.; Blanco-Brieva, G.; Fierro, J. L. G. Hydrogen Peroxide Synthesis: An Outlook beyond the Anthraquinone Process. *Angew. Chem. Int. Ed*. **2006**, *45,* 6962–6984.

(9) Taramasso, M.; Perego, G.; Notari, B. Preparation of Porous Crystalline Synthetic Material Comprised of Silicon and Titanium Oxides. *US Patent* 4 410 501, 1983.

(10) Perego*,* C.; Carati, A.; Ingallina, P.; Mantegazza, M. A.; Bellussi, G. Production of Titanium Containing Molecular Sieves and Their Application in Catalysis. *Appl. Catal. A: General* **2001**, *221*, 63–72

(11) For recent review see: Clerici, M. G.; Domine, M. E. In: *Liquid Phase Oxidation via Heterogeneous Catalysis: Organic Synthesis and Industrial Applications*; Clerici, M. G., Kholdeeva O. A. Eds.; Wiley: Hoboken, 2013; p. 21.

(12) Kholdeeva, O. A. In: *Liquid Phase Oxidation via Heterogeneous Catalysis: Organic Synthesis and Industrial Applications*; Clerici, M. G., Kholdeeva O. A. Eds.; Wiley: Hoboken, 2013; p. 127

(13) Kholdeeva, O. A.; Melgunov, M. S.; Shmakov, A. N.; Trukhan, N. N.; Kriventsov, V. V.; Zaikovskii, V. I.; Malyshev, M. E.; Romannikov, V. N. A New Mesoporous Titanium-Silicate Ti-MMM-2: a Highly Active and Hydrothermally Stable Catalyst for H_2O_2-Based Selective Oxidations. *Catal. Today* **2004**, *91-92*, 205–209.

(14) Wu, P.; Tatsumi, T.; Komatsu, T.; Yashima T. Postsynthesis, Characterization, and Catalytic Properties in Alkene Epoxidation of Hydrothermally Stable Mesoporous Ti-SBA-15. *Chem. Mater*. **2002**, *14*, 1657–1664.

(15) Xiao, F.-S. Ordered Mesoporous Materials with Improved Stability and Catalytic Activity. *Top. Catal.* **2005**, *35*, 9–24.

(16) Ivanchikova, I. D.; Kovalev, M. K.; Mel'gunov, M. S.; Shmakov, A. N.; Kholdeeva, O. A. User-Friendly Synthesis of Highly Selective and Recyclable Mesoporous Titanium-Silicate Catalysts for the Clean Production of Substituted *p*-Benzoquinones. *Catal. Sci. Technol*. **2014**, *4*, 200−207.

(17) Kholdeeva, O. A. Recent Developments in Liquid-Phase Selective Oxidation Using Environmentally Benign Oxidants and Mesoporous Metal Silicates. *Catal. Sci. Technol*. **2014**, *4*, 1869–1889.

(18) Nowak, I.; Kilos, B.; Ziolek, M.; Lewandowska, A. Epoxidation of Cyclohexene on Nb–Containing Meso- and Macroporous Materials. *Catal. Today* **2003**, *78*, 487–498.

(19) Nowak, I.; Ziolek, M. Effect of Texture and Structure on the Catalytic Activity of Mesoporous Niobosilicates for the Oxidation of Cyclohexene. *Micropor. Mesopor. Mater*. **2005**, *78*, 281–288.

(20) Somma, F.; Strukul, G. Niobium Containing Micro-, Meso- and Macroporous Silica Materials as Catalysts for the Epoxidation of Olefins with Hydrogen Peroxide. *Catal. Lett*. **2006**, *107*, 73–81.

(21) Feliczak-Guzik, A.; Nowak, I. Mesoporous Niobosilicates Serving as Catalysts for Synthesis of Fragrances. *Catal. Today* **2009**, *142*, 288–292.

(22) Gallo, A.; Tiozzo, C.; Psaro, R.; Carniato, F.; Guidotti, M. Niobium Metallocenes Deposited onto Mesoporous Silica via Dry Impregnation as Catalysts for Selective Epoxidation of Alkenes. *J. Catal*. **2013**, *298*, 77–83.

(23) Tiozzo, C.; Bisio, C.; Carniato, F.; Guidotti, M. Grafted Non–Ordered Niobium–Silica Materials: Versatile Catalysts for the Selective Epoxidation of Various Unsaturated Fine Chemicals. *Catal. Today* **2014**, *235*, 49–57.

(24) Ramanathan, A.; Zhu, H.; Maheswari, R.; Thapa, P. S.; Subramaniam, B. Comparative Study of Nb–Incorporated Cubic Mesoporous Silicates as Epoxidation Catalysts. *Ind. Eng. Chem. Res*. **2015**, *54*, 4236–4242.

(25) Ivanchikova, I. D.; Maksimchuk, N. V.; Skobelev, I. Y.; Kaichev, V. V.; Kholdeeva, O. A. Mesoporous Niobium–Silicates Prepared by Evaporation–Induced Self–Assembly as Catalysts for Selective Oxidations with Aqueous H_2O_2. *J. Catal*. **2015**, *332*, 138–148.

(26) Thornburg, N. E.; Thompson, A. B.; Notestein, J. M. Periodic Trends in Highly Dispersed Groups IV and V Supported Metal Oxide Catalysts for Alkene Epoxidation with H_2O_2. *ACS Catal.* **2015**, *5*, 5077–5088.

(27) Ivanchikova, I. D.; Skobelev, I. Y.; Maksimchuk, N. V.; Paukshtis, E. A.; Shashkov, M. V.; Kholdeeva, O. A. Toward Understanding the Unusual Reactivity of Mesoporous Niobium Silicates in Epoxidation of C=C Bonds with Hydrogen Peroxide. *J. Catal*. **2017**, *356*, 85–99.

(28) Thornburg, N. E.; Notestein, J. M. Rate and Selectivity Control in Thioether and Alkene Oxidation with H_2O_2 over Phosphonate-Modified Niobium(V)–Silica Catalysts. *ChemCatChem* **2017**, *9*, 3714–3724.

(29) Dworakowska, S.; Tiozzo, C.; Niemczyk-Wrzeszcz, M.; Michorczyk, P.; Ravasio, N.; Psaro, R.; Bogdał, D.; Guidotti, M. Mesoporous Molecular Sieves Containing Niobium (V) as Catalysts for the Epoxidation of Fatty Acid Methyl Esters and Rapeseed Oil. *J. Clean. Prod*. **2017**, *166*, 901–909.

(30) Dongare, M. K.; Singh, P.; Moghe, P. P.; Ratnasamy, P. Synthesis, Characterization, and Catalytic Properties of [Zr]-ZSM-5. *Zeolites* **1991**, *11*, 690–693.

(31) Gontier, S.; Tuel, A. Novel Zirconium Containing Mesoporous Silicas for Oxidation Reactions in the Liquid Phase. *Appl. Catal. A: General* **1996**, *143*, 125-135.

(32) Quignard, F.; Choplin, A.; Teissier. R. A Molecular Route Towards Silica Supported Zirconium Catalysts Active for the Mild Oxidation of Olefins with H_2O_2. *J. Mol. Catal. A: Chemical* **1997**, *120*, L27-L31.

(33) Besson, M.; Bonnet, M. C.; Gallezot, P.; Tkachenko, I.; Tuel, A. Catalysis for Fine Chemicals: towards Specificity with Polyphasic Media. *Catal. Today* **1999**, *51*, 547-560.

(34) Palazzi, C.; Oliva, L.; Signoretto, M.; Strukul. G. Microporous Zirconia–Silica Mixed Oxides Made by Sol–Gel as Catalysts for the Liquid-Phase Oxidation of Olefins with Hydrogen Peroxide. *J. Catal*. **2000**, *194*, 286–293.

(35) Chaudhari, K.; Bal, R.; Srinivas, D.; Chandwadkar, A. J. Sivasanker, S. Redox Behavior and Selective Oxidation Properties of Mesoporous Titano-and Zirconosilicate MCM-41 Molecular Sieves. *Micropor. Mesopor. Mater*. **2001**, *50*, 209-218.

(36) Morandin, M.; Gavagnin, R.; Pinna, F.; Strukul, G. Oxidation of Cyclohexene with Hydrogen Peroxide Using Zirconia–SilicaMixed Oxides: Control of the Surface Hydrophilicity and Influence onthe Activity of the Catalyst and Hydrogen Peroxide Efficiency. *J. Catal*. **2002**, *212*, 193–200.

(37) Wang, X.-X.; Veyre, L.; Lefebvre, F.; Patarin, J.; Basset, J.-M. Preparation and Characterization of Zirconium Containing Mesoporous Silicas. II. Grafting Reaction of Tetraneopentyl Zirconium on MCM-41 and Characterization of the Grafted Species and of the Resulting Materials. *Micropor. Mesopor. Mater*. **2003**, *66*, 169-179.

(38) Maksimchuk, N. V.; Melgunov, M. S.; Mrowiec-Białoń, J.; Jarzębski, A. B.; Kholdeeva, O. A. H_2O_2-Based Allylic Oxidation of α-Pinene over Different Single Site Catalysts. *J. Catal*. **2005**, *235*, 175-183.

(39) *Functional Metal-Organic Frameworks: Gas Storage, Separation and Catalysis*. Schröder, M., Ed. Springer-Verlag: Berlin, 2010.

(40) *Metal-Organic Frameworks: Applications from Catalysis to Gas Storage*. Farrusseng, D., Ed. Wiley: Weinheim, 2011.

(41) *Metal Organic Frameworks as Heterogeneous Catalysts*. Llabrés i Xamena, F.; Gascon, J., Eds. RCS Publishing, 2013.

(42) *Metal-Organic Frameworks: Applications in Separations and Catalysis*. García, H.; Navalón, S., Eds. Wiley-VCH Verlag: Weinheim, 2018.

(43) *Elaboration and Applications of Metal-Organic Frameworks*. Ma S., Perman J. A., Eds. World Scientific: Singapore, 2018.

(44) Hwang, Y. K.; Férey, G.; Lee, U.-H.; Chang, J.-S. in: *Liquid Phase Oxidation via Heterogeneous Catalysis: Organic Synthesis and Industrial Applications.* Clerici, M. G.; Kholdeeva O. A.; Eds. Wiley: Hoboken, New Jersey, 2013, pp. 371.

(45) Gascon, J.; Corma, A.; Kapteijn, F.; Llabrés i Xamena, F. X. Metal Organic Framework Catalysis: Quo vadis? *ACS Catal.* **2014**, *4*, 361–378.

(46) Rogge, S. M. J.; Bavykina, A.; Hajek, J.; Garcia, H.; Olivos-Suarez, A. I.; Sepúlveda-Escribano, A.; Vimont, A.; Clet, G.; Bazin, P.; Kapteijn, F.; Daturi, M.; Ramos-Fernandez, E. V.; Llabrés i Xamena, F. X.; Van Speybroeck, V.; Gascon, J., Metal–Organic and Covalent Organic Frameworks as Single-Site Catalysts. *Chem. Soc. Rev.* **2017**, *46*, 3134–3184.

(47) Yang, D.; Gates, B. C. Catalysis by Metal Organic Frameworks: Perspective and Suggestions for Future Research. *ACS Catal.* **2019**, *9*, 1779−1798.

(48) Dhakshinamoorthy, A.; Navalon, S.; Asiri, A. M.; Garcia, H. Metal Organic Frameworks as Solid Catalysts for Liquid-Phase Continuous Flow Reactions. *Chem. Commun*. **2020**, *56*, 26-45

(49) Dhakshinamoorthy, A.; Santiago-Portillo, A.; Asiri, A. M.; Garcia, H. En gineering UiO-66 Metal Organic Framework For Heterogeneous Catalysis. *ChemCatChem* **2019**, *11*, 899–923.

(50) Ye, G.; Zhang, D.; Li, X.; Leng, K.; Zhang, W.; Ma, J.; Sun, Y.; Xu, W.; Ma, S. Boosting Catalytic Performance of Metal−Organic Framework by Increasing the Defects via a Facile and Green Approach. *ACS Appl. Mater. Interfaces* **2017**, *9*, 34937−34943.

(51) Xiao, W.; Dong, Q.; Wang, Y.; Li, Y.; Deng, S.; Zhang, N. Time Modulation of Defects in UiO-66 and Application in Oxidative Desulfurization. *CrystEngComm* **2018**, *20*, 5658-5662.

(52) Viana, A. M.; Ribeiro, S. O.; de Castro, B.; Balula, S. S.; Cunha-Silva, L. Influence of UiO-66(Zr) Preparation Strategies in Its Catalytic Efficiency for Desulfurization Process. *Materials* **2019**, *12*, 3009.

(53) Limvorapitux, R.; Chen, H.; Mendonca, M. L.; Liu, M.; Snurr, R. Q.; Nguyen, S.B. T. Elucidating the Mechanism of the UiO-66-Catalyzed Sulfide Oxidation: Activity and Selectivity

Enhancements through Changes in the Node Coordination Environment and Solvent. *Catal. Sci. Technol*. **2019**, *9*, 327-335.

(54) Torbina, V. V.; Nedoseykina, N. S.; Ivanchikova, I. D.; Kholdeeva, O. A.; Vodyankina, O. V. Propylene GLycol Oxidation with Hydrogen Peroxide over Zr-Containing Metal-Organic Framework UiO-66. *Catal. Today* **2019**, *333,* 47–53.

(55) Granadeiro, C. M.; Ribeiro, S. O.; Karmaoui, M.; Valenca, R.; Ribeiro, J. C.; de Castro, B.; Cunha-Silva, L.; Balula, S. S. Production of Ultra-Deep Sulfur-Free Diesels Using a Sustainable Catalytic System Based on UiO-66(Zr). *Chem. Commun.* **2015**, *51*, 13818--13821

(56) Maksimchuk, N. V.; Lee, J. S.; Solovyeva, M. V.; Cho, K. H.; Shmakov, A. N.; Chesalov, Y. A.; Chang, J.-S.; Kholdeeva, O. A. Protons Make Possible Heterolytic Activation of Hydrogen Peroxide over Zr-Based Metal-Organic Frameworks. *ACS Catal*. **2019**, *9*, 9699−9704.

(57) Zalomaeva, O. V; Evtushok, V. Yu.; Ivanchikova, I. D.; Glazneva, T. S.; Chesalov, Yu. A.; Larionov, K. P.; O. A. Kholdeeva, Nucleophilic vs Electrophilic Activation of Hydrogen Peroxide over Zr-Based Metal-Organic Frameworks. *Inorg. Chem*. **2020**, 59, 10634–10649.

(58) Maksimchuk, N.V.; Ivanchikova, I. D.; Cho, K. H.; Zalomaeva, O. V; Evtushok, V. Yu.; Larionov, K. P.; Glazneva, T. S.; Chang, J.-S.; Kholdeeva, O. A. Catalytic Performance of Zr-Based Metal-Organic Frameworks Zr-abtc and MIP- 200 in Selective Oxidations with H_2O_2. *Chem. Eur. J.* **2021**, *27*, 6985–6992.

(59) Fournier, M.; Louis, C.; Che, M.; Chaquin, P.; Masure, D. Polyoxometallates as Models for Oxide Catalysts: Part I. An UV–visible Reflectance Study of Polyoxomolybdates: Influence of Polyhedra Arrangement on the Electronic Transitions and Comparison with Supported Molybdenum Catalysts. *J. Catal*. **1989**, *119*, 400–414.

(60) Chen, Q.; Zubieta, J. Coordination Chemistry of Soluble Metal Oxides of Molybdenum and Vanadium. *Coord. Chem. Rev*. **1992**, *114*, 107–167.

(61) Thomas, J. M. *Design and Applications of Single-site Heterogeneous Catalysts: Contributions to Green Chemistry, Clean Technology and Sustainability;* Imperial College Press: London, UK, 2012.

(62) Kholdeeva, O. A. Titanium–Monosubstituted Polyoxometalates: Relation Between Homogeneous and Heterogeneous Ti–Single–Site–Based Catalysis. *Top. Catal*. **2006**, *40*, 229–243.

(63) Kholdeeva, O. A.; Maksimovskaya, R. I. Titanium–and Zirconium–Monosubstituted Polyoxometalates as Molecular Models for Studying Mechanisms of Oxidation Catalysis. *J. Mol. Catal. A: Chem.* **2007**, *262*, 7–24.

(64) Kholdeeva, O. A. Hydrogen Peroxide Activation over Ti^{IV}: What Have We Learned from Studies on Ti-Containing Polyoxometalates? *Eur. J. Inorg. Chem*. **2013**, 1595–1605.

(65) Guillemot, G.; Matricardi, E.; Chamoreau, L.-M.; Thouvenot, R.; Proust, A. Oxidovanadium (V) Anchored to Silanol–Functionalized Polyoxotungstates: Molecular Models for Single–Site Silica–Supported Vanadium Catalysts. *ACS Catal*. **2015**, *5*, 7415−7423.

(66) Zhang, T.; Mazaud, L.; Chamoreau, L.-M.; Paris, C.; Guillemot, G.; Proust, A. Unveiling the Active Surface Sites in Heterogeneous Titanium–Based Silicalite Epoxidation Catalysts: Input of Silanol–Functionalized Polyoxotungstates as Soluble Analogues. *ACS Catal*. **2018**, *8*, 2330–2342.

(67) Solé-Daura, A.; Zhang, T.; Fouilloux, H.; Robert, C.; Thomas, C. M.; Chamoreau, L.-M.; Carbó, J. J.; Proust, A.; Guillemot, G.; Poblet, J. M. Catalyst Design for Alkene Epoxidation by Molecular Analogues of Heterogeneous Titanium-Silicalite Catalysts. *ACS Catal*. **2020**, *10*, 4737-4750.

(68) Pope, M. T. *Heteropoly and Isopoly Oxometalates*; Springer-Verlag: Berlin, 1983.

(69) *Polyoxometalate Chemistry: From Topology via Self-Assembly to Applications*; Pope, M. T., Müller, A., Eds; Kluwer: Dordrecht, 2001.

(70) Kozhevnikov, I. V. *Catalysis by Polyoxometalates;* Wiley: Chichester, 2002.

(71) Neumann, R. In: *Transition Metals for Organic Synthesis 2nd Edition*; Beller, M., Bolm, C., Eds.; Wiley-VCH: Weinheim, 2004; vol. 2, pp. 415–426.

(72) Hill, C. L. In *Comprehensive Coordination Chemistry II*; Wedd, A. G., Ed.; Elsevier Science: New York, 2004; Vol. 4, p 679–759.

(73) *J. Mol. Catal. A: Chem. Special Issue on Polyoxometalates in Catalysis;* Hill, C. L., Guest Ed.; **2007**, *262*, 1-242.

(74) Mizuno, N.; Kamata, K.; Uchida, S.; Yamaguchi, K. In Modern Heterogeneous Oxidation Catalysis: Design, Reactions and Characterization; Mizuno, N., Ed.; Wiley-VCH: Weinheim, 2009; pp. 185–217.

(75) Long, D.-L.; Burkholder, E.; Cronin, L. Polyoxometalate Clusters, Nanostructures and materials: From Self Assembly to Designer Materials and Devices. *Chem. Soc. Rev.* **2007**, *36*, 105–121.

(76) Thematic issue on Frontiers in Metal Oxide Cluster Science: Weinstock, I. A. *Israel J. Chem.* **2011**, *51*, 169−302.

(77) Themed collection on Polyoxometalate Cluster Science: Cronin, L.; Müller, A. *Chem. Soc. Rev.* **2012**, *41*, 7325−7648.

(78) Hill, C. L.; Kholdeeva, O. A. In: *Liquid Phase Oxidation via Heterogeneous Catalysis*; Clerici, M. G., Kholdeeva, O.A., Eds.; Wiley: Hoboken, New Jersey, **2013**; Ch. 6, pp. 263-319.

(79) Sun, M.; Zhang, J.; Putaj, P.; Caps, V.; Lefebvre, F.; Pelletier, J.; Basset, J.-M. Catalytic Oxidation of Light Alkanes (C_1–C_4) by Heteropoly Compounds. *Chem. Rev*. **2014**, *114*, 981−1019.

(80) Wang, S.-S.; Yang, G.-Y. Recent Advances in Polyoxometalate-Catalyzed Reactions. *Chem. Rev*. **2015**, *115*, 4893−4962.

(81) Kholdeeva, O. A. In: Frontiers of Green Catalytic Selective Oxidations; Bryliakov K. P., Ed; *Green Chemistry and Sustainable Technology*, 2019; Ch. 3, pp. 61-92.

(82) Villanneau, R.; Carabineiro, H.; Carrier, X.; Thouvenot, R.; Herson, P.; Lemos, F.; Ribeiro, F. R.; Che, M. Synthesis and Characterization of Zr (IV) Polyoxotungstates as Molecular Analogues of Zirconia-Supported Tungsten Catalysts. *J. Phys. Chem. B* **2004**, *108*, 12465-12471.

(83) Carabineiro, H.; Villanneau, R.; Carrier, X.; Herson, P.; Lemos, F.; Ribeiro, F.; Proust, A.; Che, M. Zirconium-Substituted Isopolytungstates: Structural Models for Zirconia-Supported Tungsten Catalysts. *Inorg. Chem.* **2006**, *45*, 1915-1923.

(84) Kholdeeva, O. A.; Maksimov, G. M.; Maksimovskaya, R. I.; Vanina, M. P.; Trubitsina, T. A.; Naumov, D. Yu.; Kolesov, B. A.; Antonova, N. S.; Carbó, J. J.; Poblet, J. M. Zr^{IV}-Monosubstituted Keggin-Type Dimeric Polyoxometalates: Synthesis, Characterization, Catalysis of H_2O_2-Based Oxidations, and Theoretical Study. *Inorg. Chem*. **2006**, *45*, 7224-7234.

(85) Kholdeeva, O.A.; Maksimovskaya, R.I.; Titanium- and Zirconium-Monosubstituted Polyoxometalates as Molecular Models for Studying Mechanisms of Oxidation Catalysis. *J. Mol. Catal. A: Chemical* **2007**, *262*, 7–24.

(86) Kholdeeva, O. A.; Maksimov, G. M.; Maksimovskaya, R. I.; Kovaleva, L. A.; Fedotov, M. A.; Grigoriev, V. A.; Hill, C. L. A Dimeric Titanium-Containing Polyoxometalate. Synthesis, Characterization, and Catalysis of H_2O_2-Based Thioether Oxidation. *Inorg. Chem.* **2000**, *39*, 3828-3837.

(87) Kholdeeva, O. A.; Kovaleva, L. A.; Maksimovskaya, R. I.; Maksimov, G. M. Kinetics and Mechanism of Thioether Oxidation with H_2O_2 in the Presence of Ti (IV)-substituted Heteropolytungstates. *J. Mol. Catal. A: Chem.* **2000**, *158*, 223-229.

(88) Kholdeeva, O. A.; Trubitsina, T. A.; Maksimovskaya, R. I.; Golovin, A. V.; Neiwert, W. A.; Kolesov, B. A.; López, X.; Poblet, J.-M. First Isolated Active Titanium Peroxo Complex: Characterization and Theoretical Study. *Inorg. Chem.* **2004**, *43*, 2284-2292.

(89) Kholdeeva, O. A.; Trubitsina, T. A.; Maksimov, G. M.; Golovin, A. V.; Maksimovskaya, R. I. Synthesis, Characterization, and Reactivity of Ti (IV)-Monosubstituted Keggin Polyoxometalates. *Inorg. Chem.* **2005**, *44*, 1635-1642.

(90) Kholdeeva, O. A.; Trubitsina, T. A.; Timofeeva, M. N.; Maksimov, G. M.; Maksimovskaya, R. I.; Rogov, V. A. The Role of Protons in Cyclohexene Oxidation with H_2O_2 Catalysed by Ti (IV)-Monosubstituted Keggin Polyoxometalate. *J. Mol. Catal. A: Chem.* **2005**, *232*, 173-178.

(91) Aoto, H.; Matsui, K.; Sakai, Y.; Kuchizi, T.; Sekiya, H.; Osada, H.; Yoshida, T.; Matsunaga, S.; Nomiya, K. Zirconium(IV)- and Hafnium(IV)-Containing Polyoxometalates as Oxidation Precatalysts: Homogeneous Catalytic Epoxidation of Cyclooctene by Hydrogen Peroxide. *J. Mol. Catal. A: Chem*. **2014**, 394, 224–231.

(92) Maksimchuk, N. V.; Maksimov, G. M.; Evtushok, V. Y.; Ivanchikova, I. D.; Chesalov, Y. A.; Maksimovskaya, R. I.; Kholdeeva, O. A.; Solé-Daura, A.; Poblet, J. M.; Carbo, J. J. Relevance of Protons in Heterolytic Activation of H_2O_2 over Nb(V). Insights from Model Studies on Nb-substituted Polyoxometalates. *ACS Catal*. **2018**, *8*, 9722–9737.

(93) Maksimchuk, N. V.; Ivanchikova, I. D.; Maksimov, G. M.; Eltsov, I. V.; Evtushok V. Y.; Kholdeeva, O. A.; Lebbie, D.; Errington, R. J.; Solé-Daura, A.; Poblet, J. M.; Carbó, J. J. Why does Nb(V) Show Higher Heterolytic Pathway Selectivity than Ti(IV) in Epoxidation with H_2O_2? Answers from Model Studies on Nb- and Ti-Substituted Lindqvist Tungstates. *ACS Catal*. **2019**, *9*, 6262−6275.

(94) Errington, R. J. Advanced Practical Inorganic and Metalorganic Chemistry. Blackie Academic & Professional: London, **1997**.

(95) Clegg, W.; Elsegood, M. R. J.; Errington, R. J.; Havelock, J. Alkoxide Hydrolysis as a Route to Early Transition-Metal Polyoxometalates: Synthesis and Crystal Structures of Heteronuclear Hexametalate Derivatives, *J. Chem. Soc. Dalton Trans*. **1996**, 681-690

(96) Errington R. J., Kandasamy B., Lebbie D., Izuagie T. In: Polyoxometalate-Based Assemblies and Functional Materials; Song, Y. F., Ed.; Springer: Cham., 2017; *Structure and Bonding*, Vol. 176, pp. 139-163.

(97) Harrup, M. K.; Kim, G.-S.; Zeng, H.; Johnson, R. P.; VanDerveer, D.; Hill, C. L. Triniobium Polytungstophosphates. Syntheses, Structures, Clarification of Isomerism and Reactivity in the Presence of H_2O_2. *Inorg. Chem*. **1998**, *37*, 5550–5556.

(98) Sheldon, R. A.; Kochi, J. K. *Metal–Catalyzed Oxidations of Organic Compounds, Academic Press, New York,* 1981.

(99) Jiménez-Lozano, P.; Ivanchikova, I. D.; Kholdeeva, O. A.; Poblet, J. M.; Carbó, J. J. Alkene Oxidation by Ti-Containing Polyoxometalates. Unambigous Characterization of the Role of the Protonation State, *Chem. Commun.* **2012**, *48*, 9266-9268.,

(100) Adam, W.; Haas, W.; Sieker, G. Thianthrene 5-Oxide as Mechanistic Probe in Oxygen-Transfer Reactions: the Case of Carbonyl Oxides vs. Dioxiranes. *J. Am. Chem. Soc.* **1984**, *106*, 5020−5022.

(101) Ballistreri, F. P.; Tomaselli, G. A.; Toscano, R. M.; Conte, V.; Di Furia, F. Application of the Thianthrene 5-Oxide Mechanistic Probe to Peroxometal Complexes. *J. Am. Chem. Soc.* **1991,** *113*, 6209−6212.

(102) Kholdeeva, O. A.; Kovaleva, L. A.; Maksimovskaya, R. I.; Maksimov. G. M. Kinetics and Mechanism of Thioether Oxidation with H_2O_2 in the Presence of Ti(IV)–Substituted Heteropolytungstates. *J. Mol. Catal. A: Chem.* **2000**, *158*, 223–229.

(103) Carraro, M.; Nsouli, N.; Oelrich, H.; Sartorel, A.; Sorarú, A.; Sankar Mal, S.; Scorrano, G.; Walder, L.; Kortz, U.; Bonchio. M. Reactive Zr^{IV} and Hf^{IV} Butterfly Peroxides on Polyoxometalate Surfaces: Bridging the Gap between Homogeneous and Heterogeneous Catalysis. *Chem. Eur. J.* **2011**, *17*, 8371–8378.

(104) Errington, R. J.; Petkar, S. S.; Middleton, P. S.; McFarlane, W.; Clegg, W.; Coxall, R. A.; Harrington R. W. Synthesis and Reactivity of the Methoxozirconium Pentatungstate $(nBu_4N)_6[\{(\mu\text{-}MeO)ZrW_5O_{18}\}_2]$: Insights into Proton-Transfer Reactions, Solution Dynamics, and Assembly of $\{ZrW_5O_{18}\}^{2-}$ Building Blocks. *J. Am. Chem. Soc*. **2007**, *129*, 12181–12196.

(105) DFT calculations were performed with Gaussian09 using B3LYP functional. The basis set was lanl2dz for W and Zr atoms and 6-31g(d,p) for the rest of the atoms. The solvent effects of acetonitrile were included using the IEF-PCM implicit solvation model. A data set collection of the optimized structures for the most representative species is available in the ioChem-BD repository (ref. 106) and can be accessed via DOI: 10.19061/iochem-bd-2-50. See the Supporting Information for details.

(106) Álvarez-Moreno, M.; de Graaf, C.; López, N.; Maseras, F.; Poblet, J. M.; Bo, C. Managing the Computational Chemistry Big Data Problem: The IoChem-BD Platform. *J. Chem. Inf. Model.* **2015**, *55*, 95−103.

(107) Jiménez-Lozano, P.; Carbó, J. J.; Chaumont, A.; Poblet, J. M.; Rodríguez-Fortea, A.; Wipff, G. Nature of Zr-Monosubstituted Monomeric and Dimeric Polyoxometalates in Water Solution at Different pH Conditions: Static Density Functional Theory Calculations and Dynamic Simulations. *Inorg. Chem.* **2014**, *53*, 778−786.

(108) Solé-Daura, A.; Rodríguez-Fortea, A.; Poblet, J. M.; Robinson, D.; Hirst, J. D.; Carbó, J. J. Origin of Selectivity in Protein Hydrolysis by Zr(IV)-Containing Metal Oxides as Artificial Proteases. *ACS Catal.* **2020**, *10*, 13455–13467.

(109) Jiménez-Lozano, P.; Solé-Daura, A.; Wipff, G.; Poblet, J. M.; Chaumont, A.; Carbó, J. J. Assembly Mechanism of Zr-Containing and Other TM-Containing Polyoxometalates. *Inorg. Chem.* **2017**, *56*, 4148–4156.

(110) Jiménez-Lozano, P.; Skobelev, I. Y.; Kholdeeva, O. A.; Poblet, J. M.; Carbó, J. J. Alkene Epoxidation Catalyzed by Ti-Containing Polyoxometalates: Unprecedented β‑Oxygen Transfer Mechanism. *Inorg. Chem*. **2016**, *55*, 6080−6084

(111) Donoeva, B. G.; Trubitsina, T. A.; Antonova, N. S.; Carbó, J. J.; Poblet, J. M.; Al-Kadamany, G.; Kortz, U.; Kholdeeva, O. A. Epoxidation of Alkenes with H_2O_2 Catalyzed by Dititanium-Containing 19-Tungstodiarsenate(III): Experimental and Theoretical Studies. *Eur. J. Inorg. Chem*. **2010**, 5312–5317.

(112) Skobelev, I. Y.; Zalomaeva, O. V.; Kholdeeva, O. A.; Poblet, J .M.; Carbó, J. J. Mechanism of Thioether Oxidation over Di- and Tetrameric Ti Centres: Kinetic and DFT Studies Based on Model Ti-Containing Polyoxometalates. *Chem. Eur. J.* **2015**, *21*, 14496–14506.

(113) (a) de-Azambuja, F.; Lenie, J.; Parac-Vogt, T. N. Homogeneous Metal Catalysts with Inorganic Ligands: Probing Ligand Effects in Lewis Acid Catalyzed Direct Amide Bond Formation. *ACS Catal*. **2021**, *11*, 271−277; (b) Vandebroek, L.; De Zitter, E.; Ly, G. H. T.; Conic´, D.; Mihaylov, T.; Sap, A.; Proost, P.; Pierloot, K.; Van Meervelt, L.; Parac-Vogt, T. N. Protein-Assisted Formation and Stabilization of Catalytically Active Polyoxometalate Species. *Chem. Eur. J.* **2018**, *24*, 10099 – 10108.

SYNOPSIS TOC